Maximum Power Point Tracking in Photovoltaic Systems, Using Fuzzy Logic-Based Incremental Conductance Method

趙, 宇晗
九州大学総合理工学府総合理工学専攻機械・システム理工学メジャー

Maximum Power Point Tracking in Photovoltaic Systems, Using Fuzzy Logic-Based Incremental Conductance Method

Yuhan Zhao

Supervisor

Associate Professor. Hooman Farzaneh

February 2023

Energy and Environmental Systems Laboratory,

Department of Energy and Environmental Engineering

Interdisciplinary Graduate School of Engineering Sciences

KYUSHU UNIVERSITY

Japan

Contents

List of Figures

List of Tables

Abstract

As the world economy grows, the energy demand is increasing. The use of large amounts of fossil fuels has contributed to environmental degradation. Renewable power systems have gained significant attention, as they can effectively solve the energy security problem. The most important benefit of renewable power systems is to generate electricity with zero carbon emissions, which aligns with the environmentally friendly concept of today's social development. However, renewable energies are intermittent and dependent on weather conditions, such as sunshine, wind, and operating temperature. Therefore, maximum Power Point Tracking (MPPT) is an essential technique to extract the maximum power from renewable systems, such as Photovoltaics (PVs), for the conditions at a particular instant of time.

In this research, a detailed simulation model is performed in MATLAB/Simulink, which has three parts: 1) detailed PV output electric power simulation, 2) four different MPPT methods, including two conventional methods of Perturbation and observation (P&O) and Incremental conductance (INC), one advanced intelligent method of Fuzzy logic (FLC), and one improved fuzzy logic-based variable step size INC (FL-INC), and 3) the buck-boost DC-DC converter that can be used in the system to optimize the PV output voltage, based on the duty cycle values corrected by the MPPT system.

The developed simulation model is validated using an indoor experimental system, including a solar simulator and standard test cell, and also an outdoor test setup, including three PV parallel panels with nominal power of 160 W for each, a MS-40S Pyranometer to measure the incident solar radiation on the tilted PV surface, a LM335 temperature sensor, and a data acquisitor to collect the values of current, voltage, power, and operating temperature.

Validation of the simulation results with the indoor experimental system reveals that even if the nominal power is very low, the new FL-INC method can track the maximum power faster and more accurately than other methods. Furthermore, validation of the model with the collected one-year solar incident radiation and temperature data from the outdoor test setup shows that the Fuzzy Logic control strategy can generate more than 2.04% extra power than the conventional P&O control strategy. Surprisingly, the new FL-INC method generates more energy than the FLC method and more than 2.12% power than the P&O method.

Keywords: Control strategy; Fuzzy logic; Maximum power point tracking; Photovoltaic system; DC-DC converter.

Acknowledgment

Foremost, I would like to express my sincere gratitude to my respectful supervisor, Associate Prof. Hooman Farzaneh for his continuous support, guidance, encouragement, and motivation during my whole master's research and study. He allowed me to follow this incredible energy and environmental system laboratory and do research that interests me. His mentoring helped me all the time throughout my research and thesis carefully.

Besides my supervisor, I'd like to convey my best regards to Kyushu University, which provides me with a comfortable research environment. And I am thankful to all the friendly members of the EES lab, especially Etoju Jacob, Nie Zife, Taiga Miyazaki, Alphonce, Nabeel and Rafique who gave me direct help during my study and daily life. They made my campus life colorful.

Finally, I would like to thank my parents. They support me all the time and give me the courage to go forward to make my dream come true. The support from my parents allowed me to concentrate on my research and enjoy my every day. They are the greatest of all beings in my world.

Yuhan Zhao
Kyushu University, Chikushi Campus, Fukuoka , Japan
2023. 02

Chapter 1

Introduction

1.1 Background and Literature Review

Energy plays a vital role in today's society's life and economy. The demand for fossil fuels has increased considerably since the economy has grown. In recent years, a significant increase in the demand for energy leading to a shortage of fossil fuels. Therefore, people are starting to turn their attention to renewable energy, because it can effectively solve the energy security problem [1]. Renewable energy can be harnessed from nature, such as solar, wind, biological, and waves [2]. The most significant benefit of renewable energies is to generate electricity with zero carbon emissions, which aligns with the environmentally friendly concept of today's social development.

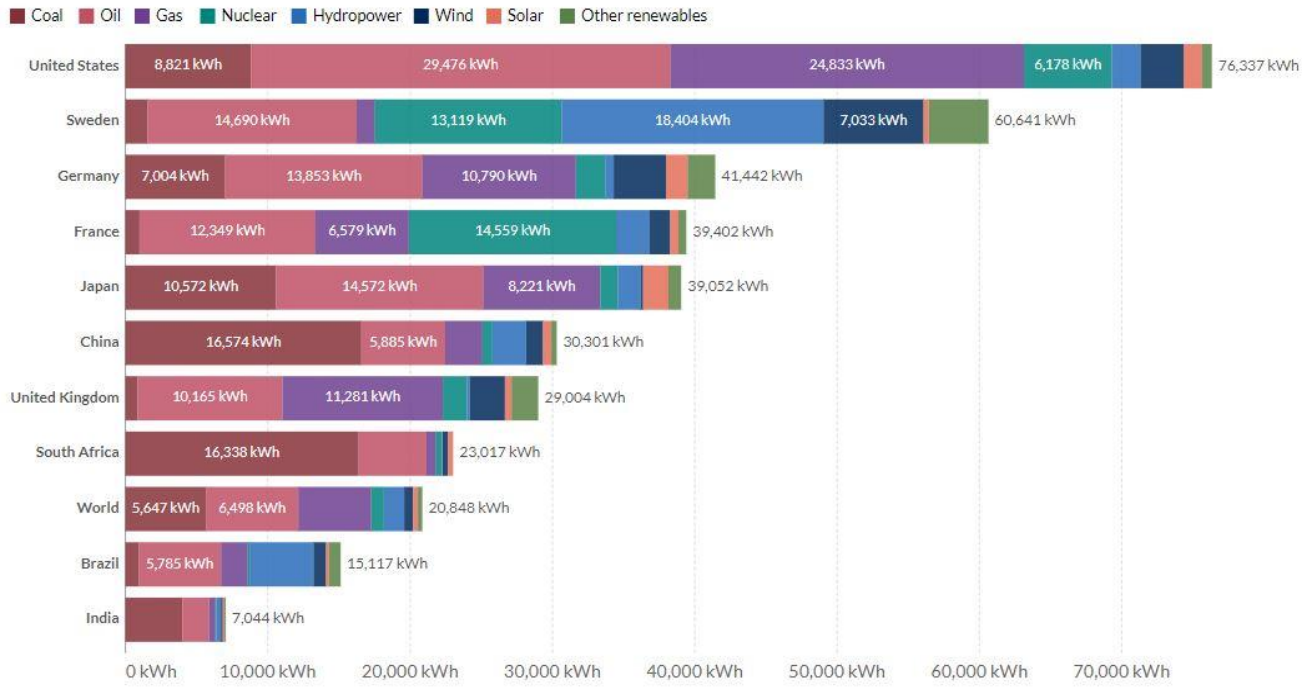

Figure 1.1. Per capita primary energy consumption (Adapted from [3]).

Figure 1.1 indicates the per capita primary energy consumption in 2021. It is not difficult to find that even in this modern society, people still have a high dependence on fossil fuels which will exacerbate environmental degradation. On the contrary, the use of renewable energy is minimal; even Photovoltaic (PV) and wind power combined are far less than oil. The use of renewable energy has become urgent.

One of the most widely used forms of renewable energy is solar energy, which can be utilized by photovoltaics to generate electricity. The principle of photovoltaic power generation is based on the semiconductor properties of the P-N junction of silicon material. The best feature of photovoltaic

electricity is that it can be generated in remote and isolated locations. With the development of technology, photovoltaics has been more widely used. Nowadays, we can find photovoltaics everywhere, such as on the home's roof and the electric light at the side of the road [4]

The output power of a solar PV varies on environmental conditions such as irregular solar irradiance, wind speed, and ambient temperature. For example, if a cloud suddenly appears in the sky and its shadow hides part of the photovoltaic panel, it can also cause unstable operation. This is one reason causes the low efficiency of PV systems. Some techniques are required to solve this problem. The maximum power point is a working point of the system where the power delivered to the load is maximized [1-4]. Based on stochastic and non-predictable features of solar irradiation, Maximum Power Point Tracking (MPPT) strategies are used to keep the operating point working at the MPP to obtain more output power in a renewable energy system. The MPPT strategies can be divided into two main groups. The first group includes classic strategies, like incremental conductance (INC) and Perturb and Observe (P&O). The second group covers intelligent strategies, like Fuzzy Logic (FLC), Artificial Neural Networks (ANN) [5].

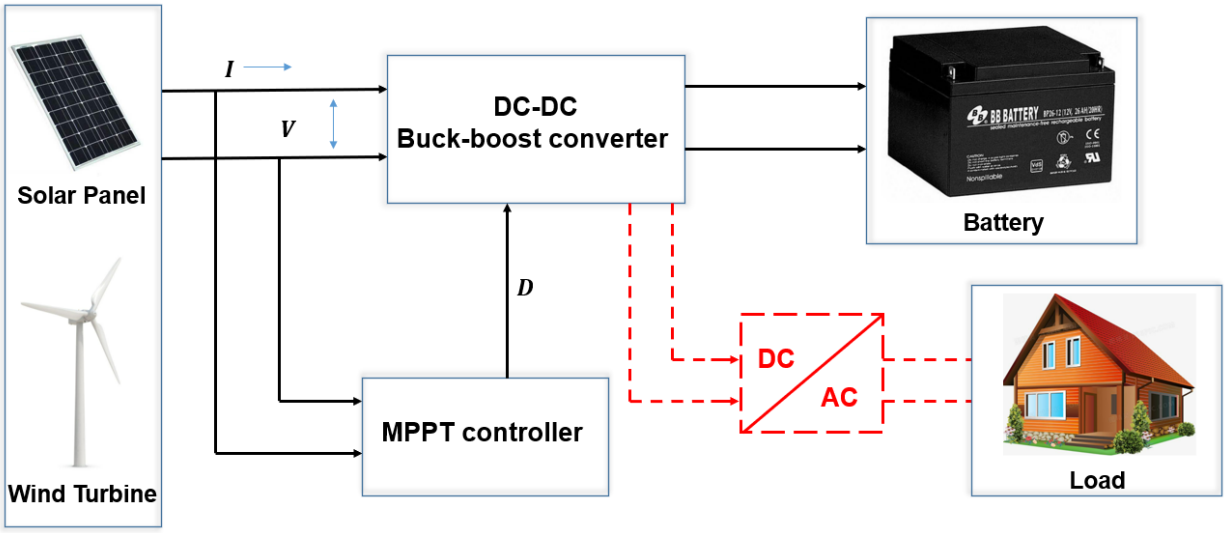

Figure 1.2. Structure of MPPT in a hybrid system.

Figure 1.2 is the typical model of MPPT. The MPPT controller receives the current and voltage from the PV module and calculates the error of the duty cycle, the new calculated duty cycle as input of the DC-DC converter, which can modify the position of the operating point. The main requirements for maximum power point tracking are simple implementation and lower cost, fast tracking speed under rapid changes in solar irradiation and temperature changes, and fewer oscillations for operating points [6].

As mentioned before, the PV or wind system output is unstable because of their operating environment. The MPPT controller will try its best to extract as much power as possible. As the desire for renewable energy study and implementation grows, interest in MPPT technology becomes even greater. There are two conventional hill climbing strategies, P&O (Perturb and Observe) and INC (Incremental Conductance), which are the two most widely used strategies in this renewable energy field. These two techniques have the advantages of simple algorithms and are easy to implement. There

is a case that P&O has been applied in one integrated stand-alone hybrid PV-wind-battery system installed in Kasuga city, Japan [7]. It verified that P&O has a good performance in controlling hybrid renewable energy systems. But the INC method is logically better than P&O. In this study, INC is proved to be easily implemented with minimal components and reduces the cost [8]. And many comparative analyses of P&O and INC have been done. In these works, the advantages and disadvantages of both methods are well explained in detail [9-10]. But classic methods have some drawbacks, such as rapid solar irradiance changes that will cause the operating point to oscillate around one of the multiple peak powers, which may cause slow tracking and fluctuation. Therefore, intelligent control strategies play a vital role in the MPPT controller. The two most common intelligent methods are Fuzzy Logic and Artificial neural networks. Most of the research applied fuzzy logic with solar and wind system. Fuzzy logic is a type of multi-valued logic that is different from P&O and INC; it is a process of uncertain human perception and cognition. Its range is not limited from 0 to 1, which makes this technique more accurate. After applying this intelligent algorithm in a renewable energy system, the operating point can track the new MPP faster and more accurately when ambient conditions change [11-13]. As previously mentioned, when the operating point of P&O and INC methods reach the MPP, it will oscillate around MPP because of their fixed step size. To solve this problem, some improved methods have been introduced. One improved P&O MPPT technique with confined search space is applied with a photovoltaic system to show its superiority. This new technique confined search space to restrict the operating point, giving a performance boost to traditional P&O methods [14]. Other research modified the INC with some techniques to make it has a variable step size. This is a fantastic solution to the fluctuation problem, which gives the operating point a more stable and faster-tracking speed [15-16]. Table 1.1 shows the recent MPPT strategies for photovoltaic and wind systems.

Table 1.1. A review of recent MPPT strategies for PV and wind systems.

Configuration	**Energy Sources**	**MPPT strategies**	**Converter type**	**Ref**
Stand-alone	Hybrid PV-wind-battery	Perturb and Observe (P&O)	Buck converter	[7]
Stand-alone	Photovoltaic	Incremental Conductance (INC)	Buck-boost converter	[8]
Stand-alone	Photovoltaic	Fuzzy Logic (FLC)	Buck converter	[12]
Stand-alone	Photovoltaic	Fuzzy Logic (FLC)	Buck-boost converter	[13]

Stand-alone	Photovoltaic	Improved P&O	Boost converter	[14]
Stand-alone	Photovoltaic	Improved INC	Boost converter	[17]
Stand-alone	Hybrid PV-wind-battery	Artificial Neural Networks (ANN)	Boost converter	[18]

1.2 What will be elucidated in this research

This study aims to introduce a novel MPPT technique based on a combination of fuzzy logic (FLC) and incremental conductance (INC) methods to extract output power from photovoltaic systems at a higher MPP with faster tracking. The first part of this study focuses on detailed dynamic simulating work with different MPPT methods. In this novel method, fuzzy logic is used to produce a variable step size for INC that solves the problem caused by the fixed steps in this method. The proposed MPPT will be tested in outdoor and indoor experimental systems to prove its high accuracy and stability compared to other traditional and commercial methods.

The rest of the thesis is organized as follows: Chapter 2 covers four different MPPT methods, including Perturb and Observe (P&O), Incremental Conductance (INC), Fuzzy Logic (FLC), and Fuzzy logic based INC (FL-INC). This section explains the principles, advantages and disadvantages of these methods in detail. In Chapter 3, the mathematical model of photovoltaic output is introduced in detail first, then the DC-DC converter is presented, especially the mathematical model and parameters' calculation of buck-boost DC-DC converter. The simulation model used in this study is also carried out to compare different MPPT methods' performance at standard testing conditions (STC) in this chapter. Chapter 4 includes indoor experimental system validation and simulation results, taking into account a real case study of a PV module with nominal power 480W whose input data was collected by the outdoor experimental device installed in Chikushi campus, Kyushu University. Finally, chapter 5 concludes the research of more efficient maximum power point tracking techniques with a brief addition of future work.

Chapter 2

Maximum Power Point Tracking techniques

2.1. Perturb and Observe method (P&O)

The Perturb and Observe (P&O) method is a conventional hill climbing method. In this algorithm, the operating point is always perturbed, even if it is close to the MPP. The controller compares the voltage and power of the operating point at sample time (K) with sample time (K-1) to forecast the perturbing direction. As shown in Figure 2.1. It has a fixed step size. If the operating point worked at the left side of MPP, that means with voltage increasing ($dP > 0$), the changed value of power output is also greater than 0 ($dP > 0$), and the voltage perturbation is continued in the same direction. If in this perturbation direction that gives a negative response ($dP < 0$), the perturbation should be opposite [19].

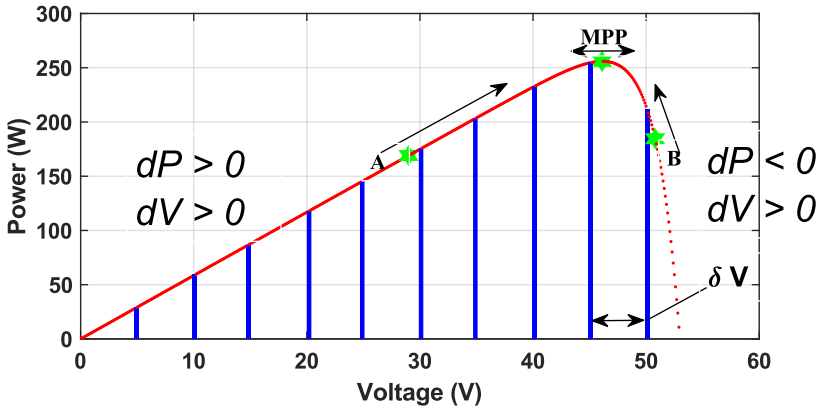

Figure 2.1. PV power-voltage characteristic curve.

Figure 2.2 shows the flow chart of Perturb and Observe method. In the P&O method, if the operating point at the left side of MPP produces a signal to reduce the duty cycle of the DC-DC converter to bring the operating point close to MPP. On the contrary, if the operating point exceeds the MPP operating on the right side, the duty cycle will be increased to decrease the operating point's voltage to prohibit it from moving further to the right.

However, some drawbacks exist in the P&O method, such as slow tracking speed. When dramatic solar radiation or temperature changes happen, the operating point will fluctuate around one of the local peak powers because of its fixed step size. But as a traditional MPPT method, it is still one of the most commonly used methods.

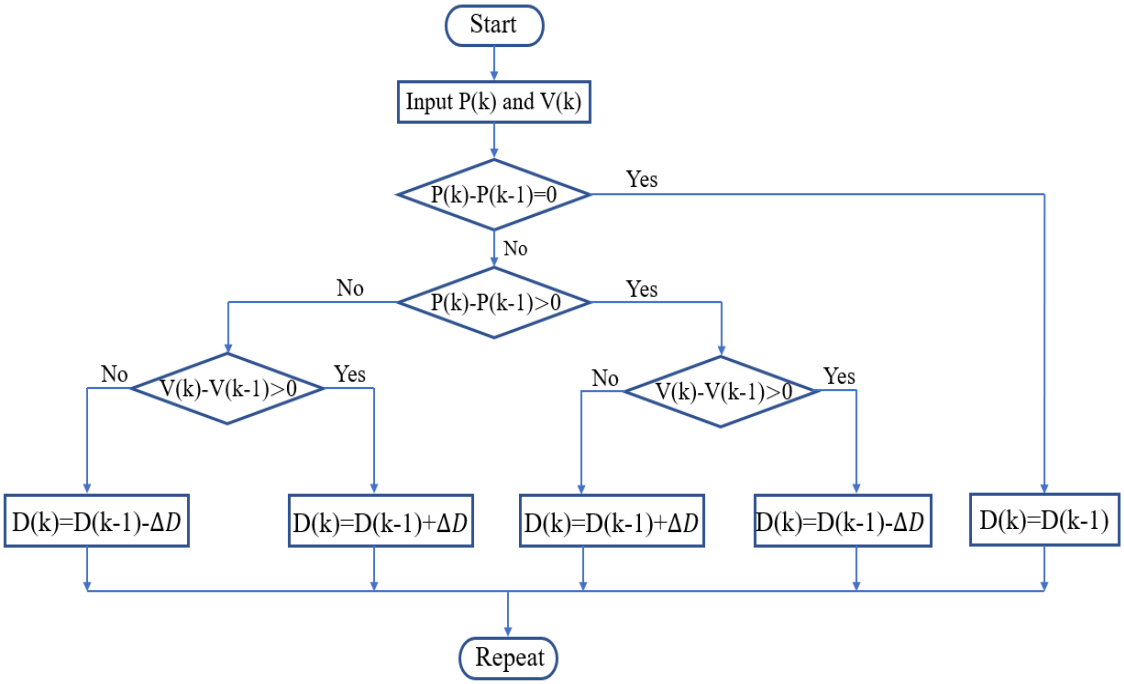

Figure 2.2. P&O algorithm flow chart.

2.2. Incremental Conductance method (INC)

The Incremental Conductance (INC) method compares the conductance (I/V) of the PV system with its partial derivative (dI/dV) to find the maximum power point. The real-time location of the operating point is estimated by the following equations [20]:

$$\frac{dI}{dV} = -\frac{I}{V}\ , \quad At\ the\ MPP \tag{2.1}$$

$$\frac{dI}{dV} > -\frac{I}{V}\ , \quad At\ the\ left\ side\ of\ the\ MPP \tag{2.2}$$

$$\frac{dI}{dV} < -\frac{I}{V}\ , \quad At\ the\ right\ side\ of\ the\ MPP \tag{2.3}$$

Figure 2.3 is the flow chart of the Incremental Conductance method, which describes the algorithm in detail. If $(dI/dV) > (-I/V)$, the voltage of the operating point should be increased. If $(dI/dV) < (-I/V)$, the duty cycle should be increased. If $dV = 0$, the value of dI should be compared with 0.

This INC method is theoretically superior to P&O. However, the tracking speed of INC is not fast enough due to its fixed step size. The fluctuations would be eliminated theoretically when the operating point work at MPP, but it is difficult because it's a fixed step. There is an improved method that can solve this problem will be introduced in the next subsection. Although this method has some drawbacks, it is still one of the most widely used methods in the industry.

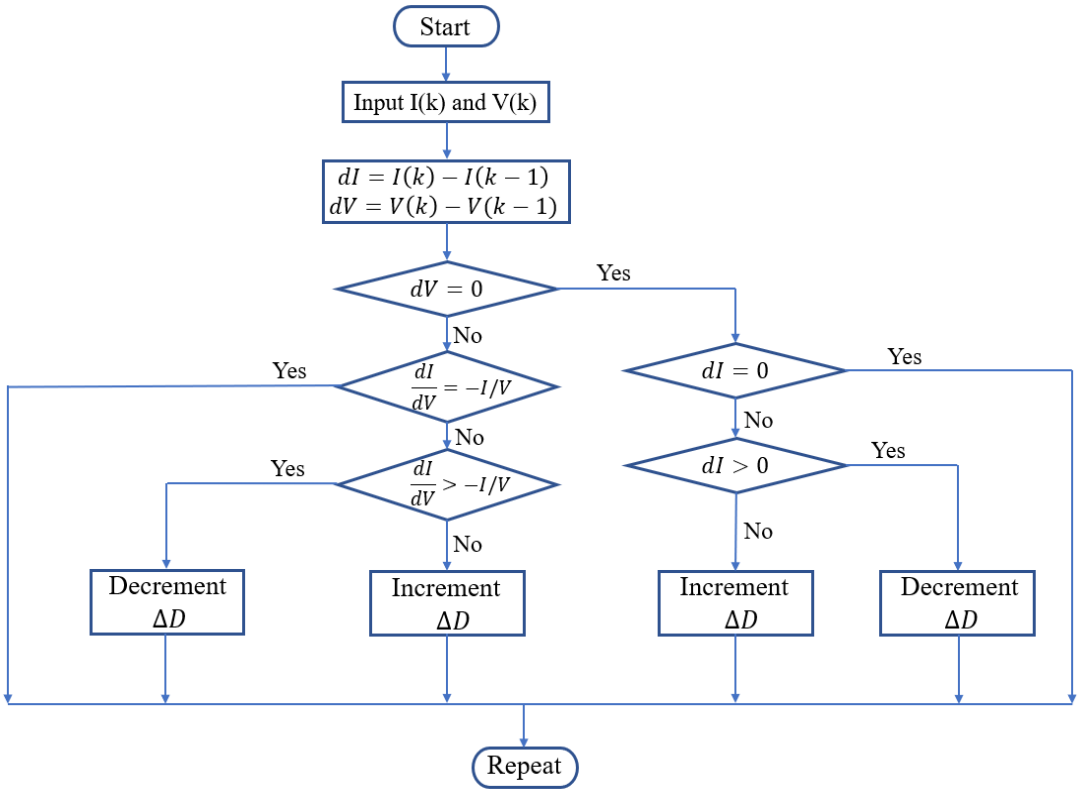

Figure 2.3. INC algorithm flow chart.

2.3. Fuzzy Logic Control method (FLC)

Fuzzy logic appeared in the fuzzy set background proposed by Lotfi Asker Zadeh [21]. This is a multi-valued logic whose value is not limited from 0 to 1, like human perception and cognition processes are uncertain. The most important features in this logic are fuzzy rules and membership functions. In conventional logic, a 0 means “totally false” or a 1 means “totally true”. But in fuzzy logic, a fuzzy set assigns a degree of membership, which can express ambiguities more accurately. A fuzzy logic controller includes four main components: fuzzification interface, knowledge base (database and rule base), decision-making unit, and defuzzification interface. These components and the general structure of a FLC are shown in Figure 2.4.

The fuzzification interface transforms the numerical inputs into fuzzy inputs based on fuzzy rules and membership functions. After this step, input variables become linguistic variables that can express changed values more accurately and be recognized by the decision-making unit. Finally, the expected crisp output is derived by defuzzification techniques. One of the most commonly used defuzzification methods is Centroid Method.

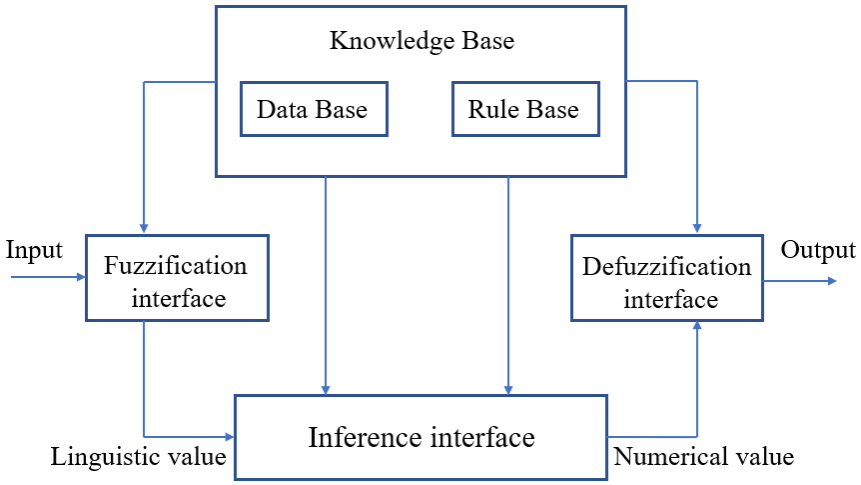

Figure 2.4. Structure of fuzzy logic controller.

The fuzzy logic controller has been widely used in renewable energy systems. The applications of the fuzzy logic controller have increased in recent years because of its highly robust.

There are two inputs: error $E(k)$ and changed value of error $CE(k)$ that correspond to the operating point tangential slope on the P-V curve and movement direction of the operating point; both of them can help us estimate the position of the operating point. The expression of $E(k)$ and $CE(k)$ are shown in equations (2.4) and (2.5) as follows [12]:

$$E(k) = \frac{P(k) - P(k-1)}{V(k) - V(k-1)} = \frac{\Delta P}{\Delta V} \tag{2.4}$$

$$CE(k) = E(k) - E(k-1) = \Delta E \tag{2.5}$$

The output of FLC $\Delta D(k)$ is a variation of the duty cycle, which is responsible for adjusting the duty cycle of the DC-DC converter in order to track the MPP of the PV system [12]. An accumulator has been made to calculate the value of the duty cycle in equation (2.6):

$$D(k) = D(k-1) + \Delta D(k) \tag{2.6}$$

Where, k is the sample time.

Triangular membership functions are used for inputs and output. They have a different universe of discourse. Figure 2.5, 2.6, and 2.7 shows the detail of the membership function for inputs and output.

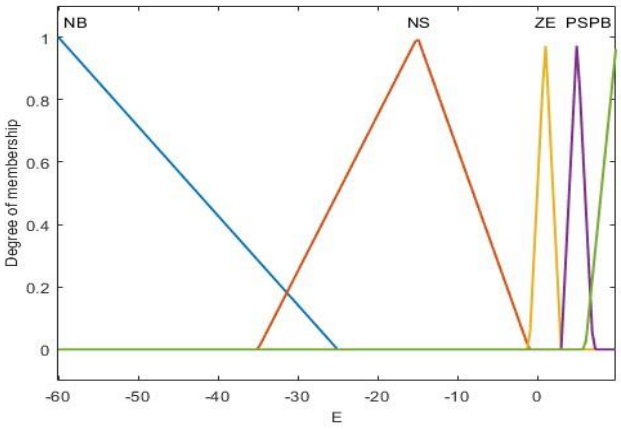

Figure 2.5. Membership function of $E(k)$.

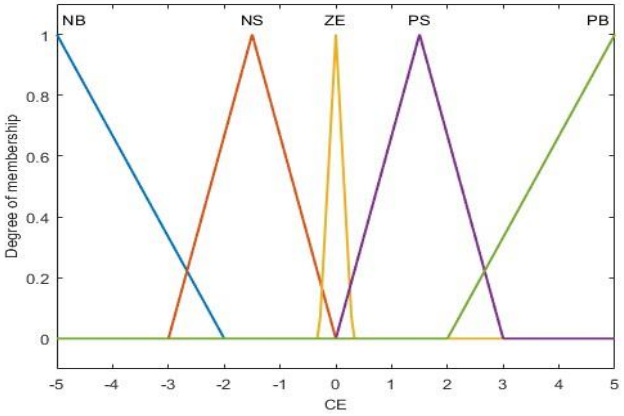

Figure 2.6. Membership function of $CE(k)$.

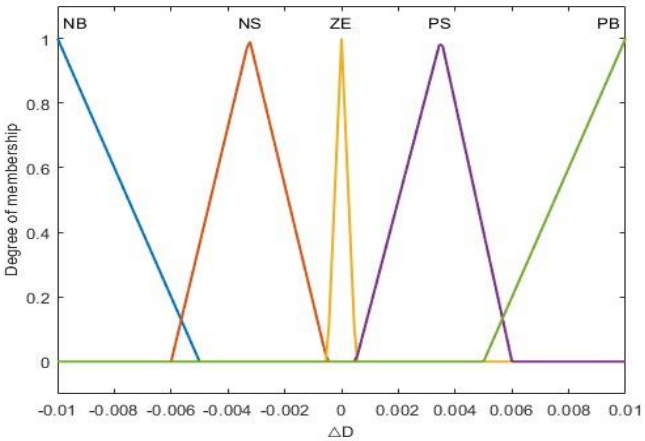

Figure 2.7. Membership function of $\Delta D(k)$.

According to the figures above, the universe of discourse for $E(k)$ is (-60 to 10), (-5 to 5) for $CE(k)$, and (-0.01 to 0.01) for $\Delta D(k)$. There are five linguistic labels for input variables and output variables: Negative Big (NB), Negative Small (NS), Zero (ZE), Positive Small (PS), and Positive Big (PB). Table 2.1 displays the 25 fuzzy rules used for the PV system.

Table 2.1. Fuzzy rules for the PV system.

		CE				
		NB	NS	ZE	PS	PB
E	NB	ZE	PB	PB	PB	PB
	NS	PB	PB	PS	ZE	ZE
	ZE	PS	ZE	ZE	ZE	NS
	PS	ZE	ZE	NS	NB	NB
	PB	ZE	NB	NB	NB	ZE

While applying these five linguistic labels on P-V characteristic curve, the P-V curve can also be divided into five regions like Figure 2.8. In regions PB and PS, $E(k)$ is positive, which means the operating point is working at the left side of MPP. For example, if $E(k)$ is PS and $CE(k)$ is also PS indicates the operating point is getting away from MPP to the left side. At this condition, FLC produces NB to reduce the duty cycle and move the OP towards MPP. In region ZE, the operating point is very close to MPP. In regions NS and NB, when $E(k)$ is negative but $CE(k)$ is positive, it means OP is moving towards MPP from the right side. So the fuzzy controller output is ZE or PB to accelerate its approach to the MPP.

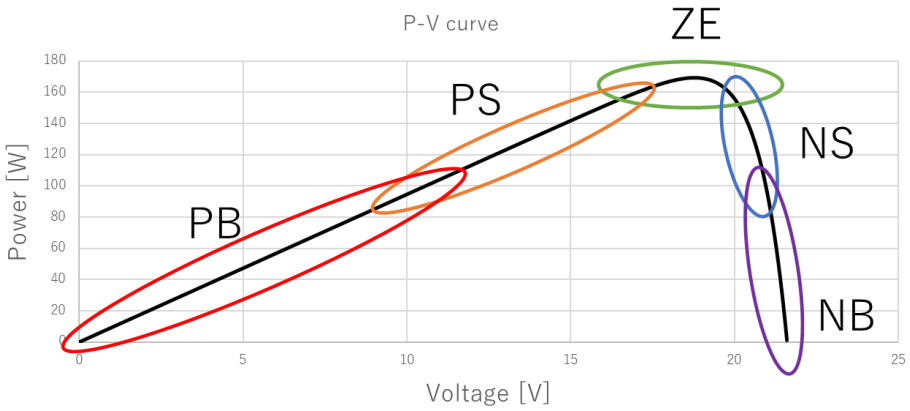

Figure 2.8. P-V curve divided into five regions.

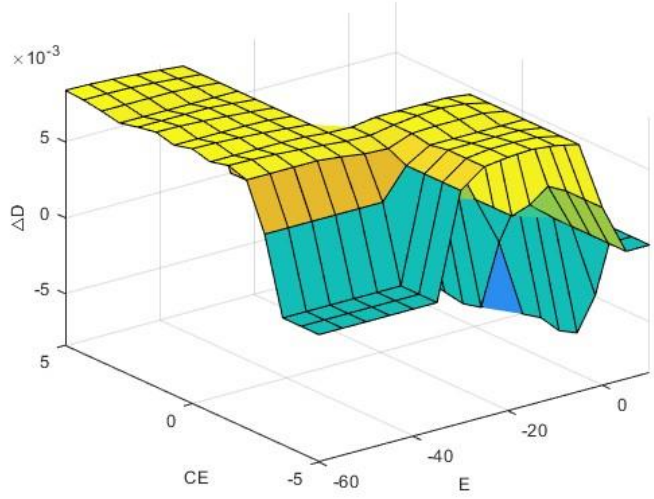

Figure 2.9. Surface view of fuzzy logic used in PV.

Figure 2.9 shows the 3D fuzzy surface waveform of FLC for two inputs $E(k)$, $CE(k)$, and output $\Delta D(k)$. It shows more intuitively the changing pattern of fuzzy rules. If any change occurs in the given inputs, the output can automatically be found according to the input change.

2.4. Fuzzy logic-based Incremental Conductance (FL-INC)

The most widespread MPPT techniques are Perturb and Observe (P&O) and Incremental Conductance (INC). Recently, many researchers have considered how to improve the performance of P&O, and some unique methods have been formed. Such as, some techniques are used to vary the step size of P&O or improve its tracking speed. And these new technically improved P&O methods have a significant performance improvement.

INC is also popular because its logic is superior. But the conventional INC algorithm consists of some division computations that demand a stronger microcontroller, including high frequency and large memory. It will cost a lot of money to implement [22]. Furthermore, the operating point will oscillate around MPP with the INC method due to its fixed step size, which will decrease tracking efficiency. To solve this problem, a novel fuzzy-logic-based INC (FL-INC) will be introduced in this research. The structure of the load-connected PV array with the fuzzy-logic-based variable step size INC is shown in Figure 2.10.

There are two inputs for the fuzzy-logic-based INC: the instantaneous conductance (I/V) and the changed value of instantaneous conductance (dI/dV). And the desired output is the variable voltage step size reflected by the variable duty cycle step size applied to change the duty cycle of the DC-DC converter. The characteristic I-V curve and P-V curve can be divided into five regions according to their positions with respect to the maximum power point [23]. If $dP/dV \gg 0$, $I/V \gg -dI/dV$, which means the voltage of the operating point is much lower than the voltage of MPP from the left side, the proper voltage step size is positive big (PB). If $dP/dV > 0$, $I/V > -dI/dV$, which means the voltage

of the operating point is a little lower than the MPP voltage at the left side of the MPP, the suitable step size should be positive small (PS). If $dP/dV \approx 0, I/V \approx -dI/dV$, the OP is very close to the MPP, so the step size needs to be very small (VS). And vice versa. According to the characteristics of the INC method, fuzzy rules for producing the suitable variable step duty cycle of FL-INC can be shown below in Table 2.2.

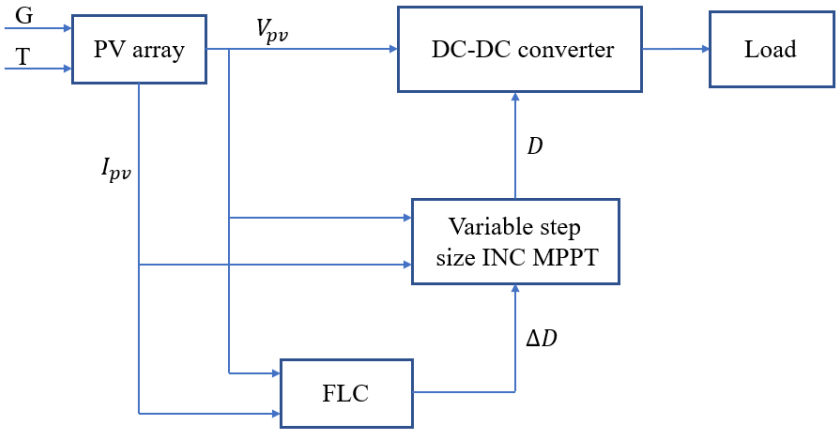

Figure 2.10. Structure of variable step size FL-INC.

Table 2.2. Fuzzy rules for generating the variable step duty cycle [23].

		dI/dV				
		VL	L	VC	H	VH
I/V	VL	PB	PS	PS	VS	NS
	L	PB	PS	VS	NS	NB
	VC	PB	PS	VS	NS	NB
	H	PB	PS	VS	NS	NB
	VH	PB	PS	PS	NS	NB

The important membership functions of inputs and output are shown in Figures 2.11, 2.12, and 2.13. The fuzzy inputs and output have been carefully designed at specific conditions [23]. When the solar irradiance and temperature change, the effective value for inputs and output will change.

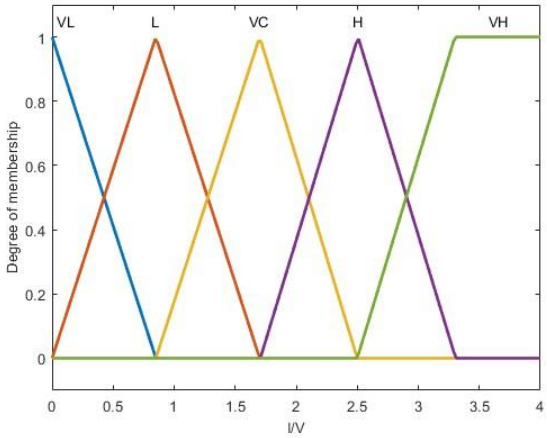

Figure 2.11. Membership function of I/V.

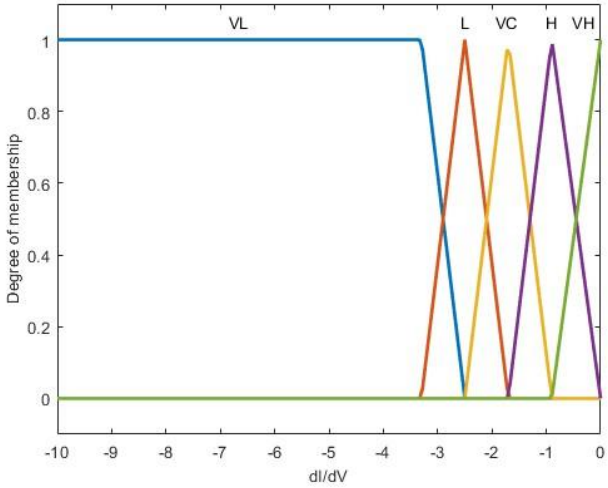

Figure 2.12. Membership function of $dI/\mathrm{d}V$.

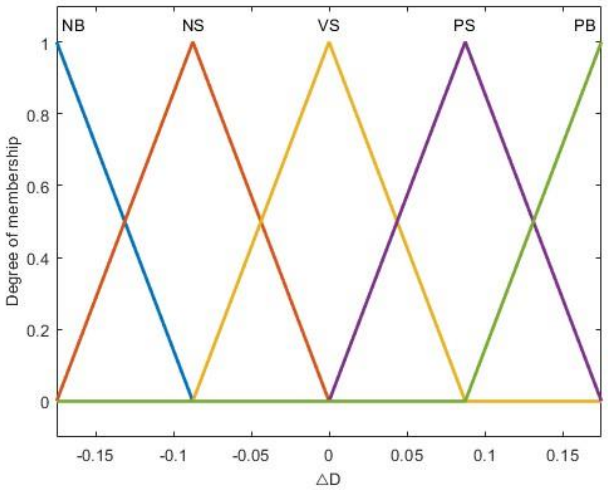

Figure 2.13. Membership function of ΔD.

This unique fuzzy logic-based INC method has an outstanding performance that will be demonstrated in the next chapter. This method not only enhances output DC power and has more minor fluctuations but also reduces the convergence time to reach the steady-state condition with instantly variable weather conditions. In the next chapter, this method will be applied for the first time connecting to the buck converter with minor adjustments.

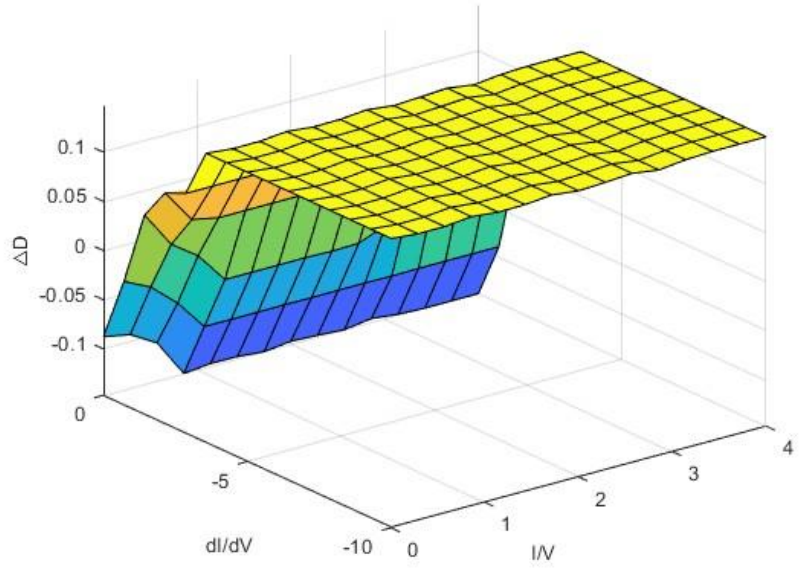

Figure 2.14. Surface view of FL-INC used in PV.

Figure 2.14 shows the 3D fuzzy surface waveform of FL-INC for two inputs I/V, dI/dV and output $\Delta D(k)$. It shows more intuitively the changing pattern of fuzzy rules. If any change takes place in the given inputs, the output can automatically be found according to the change in the inputs.

Chapter 3

MPPT Simulation Model

3.1. Principle of Photovoltaic (PV) system

One PV module consists of many solar cells; the main components of a solar cell are n-type silicon and p-type silicon [24]. The basic concept circuit is shown in Figure 3.1. Due to material properties and special processes, n-type silicon has many free electrons (negative), but p-type silicon has many holes (positive). When two materials come into contact with each other, a concentration difference of electrons and holes is created at the contact surface. As a result, some electrons move from n-type silicon to p-type silicon, and holes move from p-type to n-type silicon. Then, an internal electric field is formed inside the two materials, with the direction of this electric field pointing from n-side to p-side that, preventing diffusion movements due to concentration differences. When the solar radiation reaches the surface of the PV cell, the electrons are excited, moving towards the n-side, the holes move in the opposite direction, and eventually, the n-type silicon becomes a negative electrode of the external circuit.

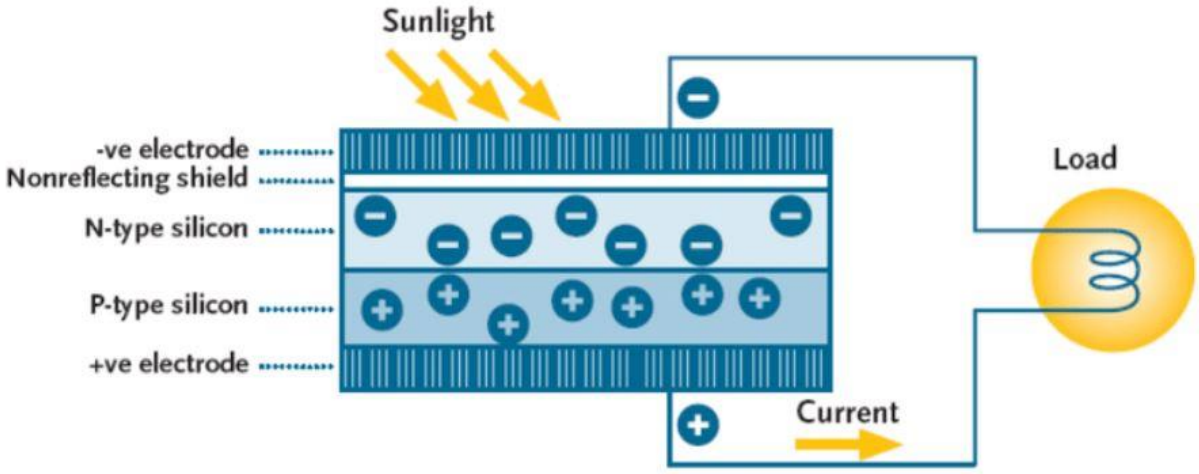

Figure 3.1. Basic concept of the solar cell (Adapted from [25]).

3.2 Mathematical model of PV

The solar cell is a semiconductor device that converts sunlight energy into electricity. Figure 3.2 represent the single-diode equivalent model of a PV cell. It includes a series resistor and a shunt resistor.

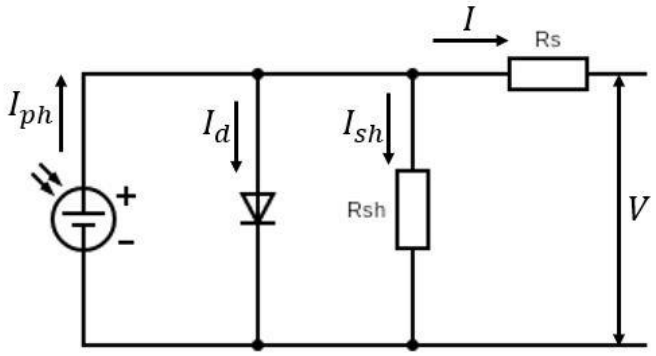

Figure 3.2. Equivalent circuit of the single-diode PV cell.

For drawing the electrical characteristic curve of the PV system, according to Kirchhoff's current law (KCL) the following equations are used [7]:

$$I = I_{ph} - I_d - I_{sh} \tag{3.1}$$

Where I is the output current of solar module (A), I_{ph} is the current source of the solar module by irradiance (A), I_d is current of the diode (A) and I_{sh} is the leakage current across the parallel resistor (A). The photocurrent produced by cell I_{ph} is expressed by the following equation [26]:

$$I_{ph} = I_{sc} \times \left(1 + K_i \times (T_a - T_n)\right) \times \frac{G}{G_n} \tag{3.2}$$

Where:
I_{sc}: short circuit current at standard conditions (A)
K_i: temperature coefficient of I_{sc} [0.00175 (A/K)]
T_a: given temperature of the cell (K)
T_n: cell temperature at STC (298 K)
G: solar irradiance on the cell surface (W/m^2)
G_n: nominal value of irradiance (W/m^2)

The current of the diode is expressed as follows:

$$I_d = I_0 \times \left(e^{\frac{V_d}{V_T}} - 1\right) \tag{3.3}$$

The reverse saturation current of the diode I_0 is calculated by:

$$I_0 = I_{on} \times \left(\frac{T_a}{T_n}\right)^3 \times e^{\frac{q \times E_g}{A \times K} \times \left(\frac{1}{T_n} - \frac{1}{T_a}\right)} \tag{3.4}$$

I_{on} is the reverse saturation current of the diode at reference temperature:

$$I_{on} = \frac{I_{sc}}{e^{\frac{q \times V_{oc}}{A \times K \times T_n}} - 1} \tag{3.5}$$

Where:
q: electric charge of the electron ($1.60 \times 10^{-19} C$)
E_g: material band gap [1.12 (25℃)]
A: ideality factor of the diode (value range from 1 to 2)
K: Boltzmann constant ($1.38 \times 10^{-23} J/K$)
V_{oc}: open circuit voltage at normal condition (V)

In equation (3.3), V_d is the voltage across the diode and V_T is expressed as below:

$$V_T = \frac{KT_a}{q} \times A \times N_s \tag{3.6}$$

$$V_d = V + I \times R_s \tag{3.7}$$

Where N_s is the number of cells, R_s is series resistance. The leakage current going through the shunt resistor I_{sh} can be calculated as:

$$I_{sh} = \frac{(V + IR_s)}{R_{sh}} \tag{3.8}$$

R_{sh} is the value of shunt resistance.

Combining the equations above, the output current of the PV module is:

$$I = I_{ph} - I_0 \left[e^{\frac{q(V+IR_s)}{AKT_aN_s}} - 1 \right] - \frac{(V + IR_s)}{R_{sh}} \tag{3.9}$$

To present this mathematical model of the photovoltaic system more clearly and intuitively, a flowchart is made in Figure 3.3:

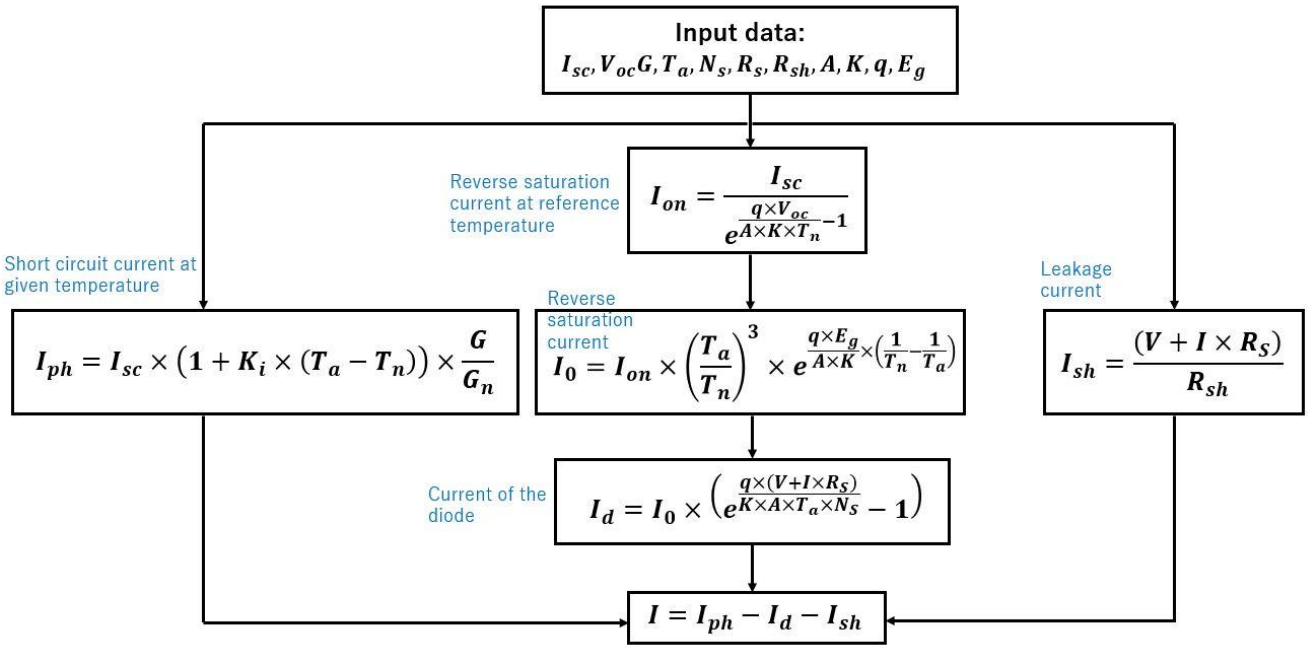

Figure 3.3. Flowchart of PV's mathematical model

Table 3.1 shows the electrical data of Panasonic's photovoltaic module type VBHN245SJ25, which is used to test the developed mathematical model. The characteristic I-V curve of the panel is shown in Figure 3.4.

Figure 3.5 represents the characteristic I-V curve extracted from using the developed model Panasonic PV module.

Table 3.1. Electrical data of Panasonic's type VBHN245SJ25 PV module

Number of cells (N_s)	72
Maximum power (P_{max})	245 [W]
Maximum power voltage (V_{mp})	44.3 [V]
Maximum power current (I_{mp})	5.54 [A]
Open circuit voltage (V_{oc})	53.0 [V]
Short circuit current (I_{sc})	5.86 [A]
Series resistance (R_s)	0.0001 [Ω]
Shunt resistance (R_{sh})	1000 [Ω]

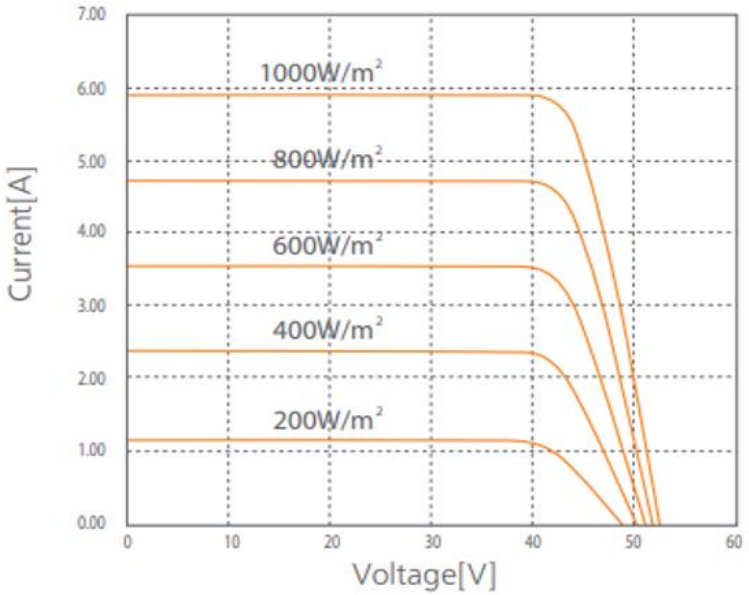

Figure 3.4. Characteristic I-V curve of selected Panasonic PV module.

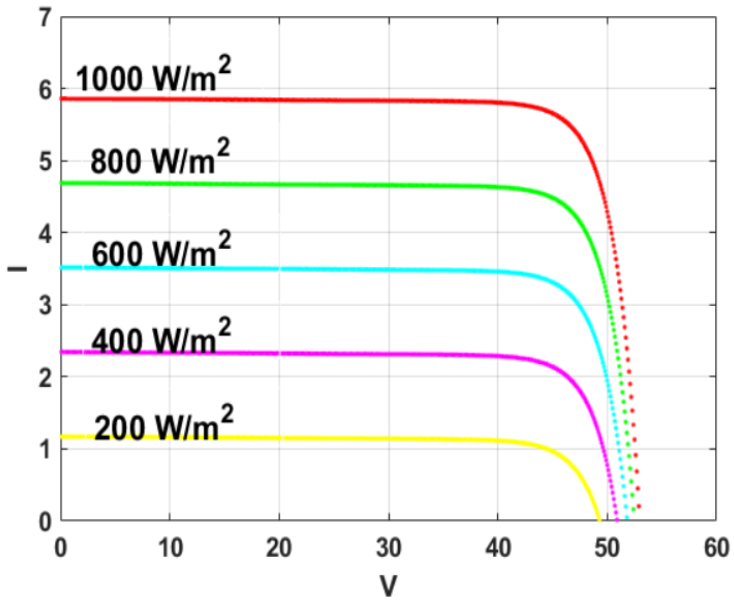

Figure 3.5. Simulation result of MATLAB code.

Comparing the MATLAB simulation result with I-V characteristic curve given by the Panasonic panel with solar radiation range from 200W/m^2 to 1000W/m^2, it can be observed that, the characteristic I-V curves of the simulation result are generally consistent with the given I-V curve by the Panasonic manufacturer.

3.3. DC-DC converter introduction

There are three common DC-DC converters: buck converter, boost converter, and buck-boost converter. They are introduced below:

3.3.1 Buck DC-DC converter

As its name suggests, the main function of a buck converter is to step down the voltage. The structure of the buck converter is shown in Figure 3.6, which is composed of one switch, one diode, one inductor, and one capacitor. The output voltage of this kind of converter is lower than the input voltage. The relationship between the output voltage and the input voltage is shown in equation (3.10).

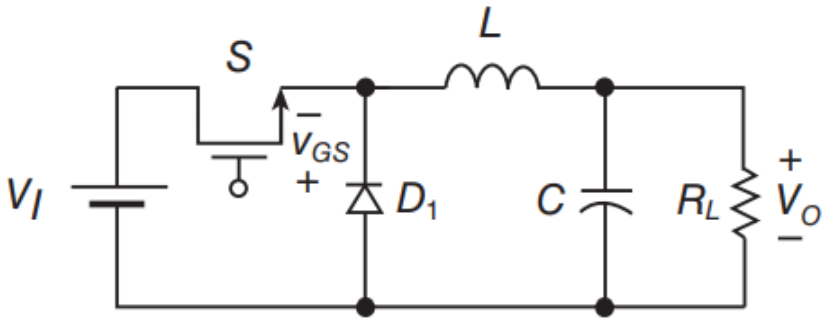

Figure 3.6. Structure of buck converter (Adapted from [27]).

$$V_o = D \times V_i \tag{3.10}$$

Where:

V_o: Output voltage (V)

V_i: Input voltage (V)

D: Duty cycle

The principle of the buck converter is when the switch is on, current flows through the inductor, and electrical energy is converted into magnetic energy and stored in the inductor. When the switch is turned off, the energy stored in the inductor is converted to electricity supplied to the load as the source that can decrease the voltage. This type of converter is used for the circuit whose load demand voltage is lower than the input voltage; it is widely used in renewable energy modeling.

3.3.2. Boost DC-DC converter

It is different from a buck converter; the main function of a boost converter is to step up the voltage. The structure of the boost converter is shown in Figure 3.7, which has the same number of switches, diode, inductor, and capacitor as the buck converter but configurated differently. As a result, the output voltage of this kind of converter is higher than the input voltage. The relationship between the output and input voltage is shown in equation (3.11).

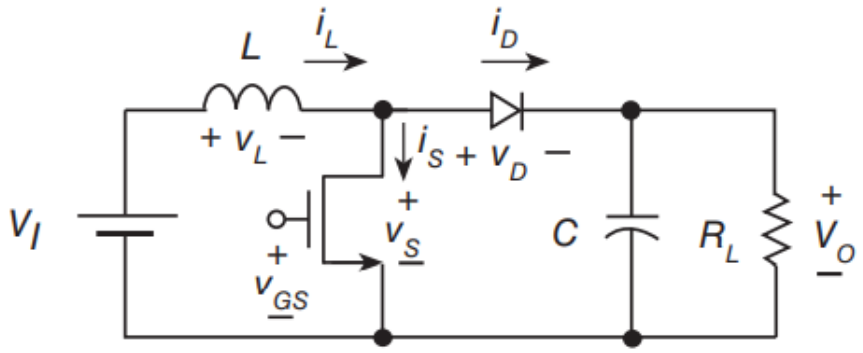

Figure 3.7. Structure of boost converter (Adapted from [27]).

$$V_o = \frac{V_i}{(1-D)} \tag{3.11}$$

The principle of the buck converter is when the switch is on, and current flows through the inductor, electrical energy is converted into magnetic energy and stored in the inductor. At the same time, the capacitor supplies electricity to the load. When the switch is turned off, the diode is conducted, and the energy stored in the inductor is converted into electricity supplied to the capacitor and the load. The capacitor supplies the energy to load continuously. As a result, the output voltage becomes higher than the input voltage. This type of converter is used for the circuit whose load demand voltage is higher than the input voltage, and it is also widely used in renewable energy modeling.

3.3.3. Buck-boost DC-DC converter

The conventional buck-boost converter has the same number of components as the buck or boost converter. The buck-boost converter not only can step up, but also step down the voltage. It can be considered as a buck converter connected with a boost converter in series. The structure of the buck-boost converter is shown in Figure 3.8. The relationship between the output and the input voltage is shown in equation (3.12).

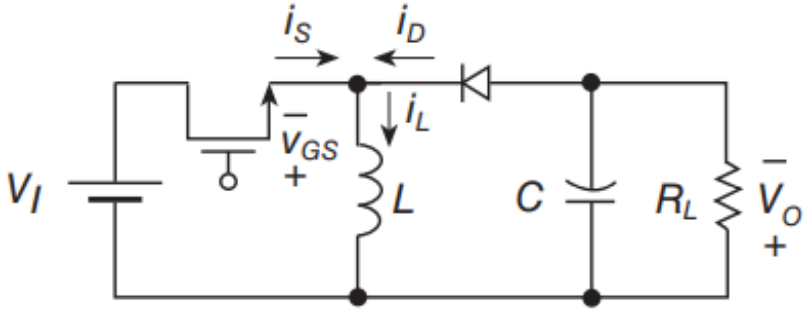

Figure 3.8. Structure of buck-boost converter (Adapted from [27]).

$$V_o = -V_i \times (\frac{D}{1-D}) \tag{3.12}$$

The output voltage of a conventional buck-boost converter has the opposite polarity if the number of components is the same as the simple buck or boost converter. The reason is explained below:

In the positive volt-second of the inductor (T_{on}):

$$V_i \times T_{on} \tag{3.13}$$

In the reverse volt-second of the inductor (T_{off}):

$$-V_o \times (T - T_{on}) \tag{3.14}$$

Combining equations (3.13) and (3.14), the opposite polarity output of the buck-boost converter can be clarified. However, because of the negative output voltage, the use of a buck-boost converter is limited. Although the buck converter was selected to control the output voltage in this previous research, it can only step down the input voltage. The advantage of a buck-boost converter is not only that the voltage can be stepped up or down as required, but also it can handle a wide range of input voltage, which is more suitable for solar energy.

3.3.4. Mathematical model of the buck-boost converter:

Mathematical modeling of the buck-boost DC-DC converter is one of the basic subjects in the analysis of its performance. There is a comprehensive mathematical model which is able to obtain the values of inductor current and output voltage in each instant of the time [28]. In order to make the whole complex mathematical model look more intuitive, the flow chart is made in Figure 3.9. as below:

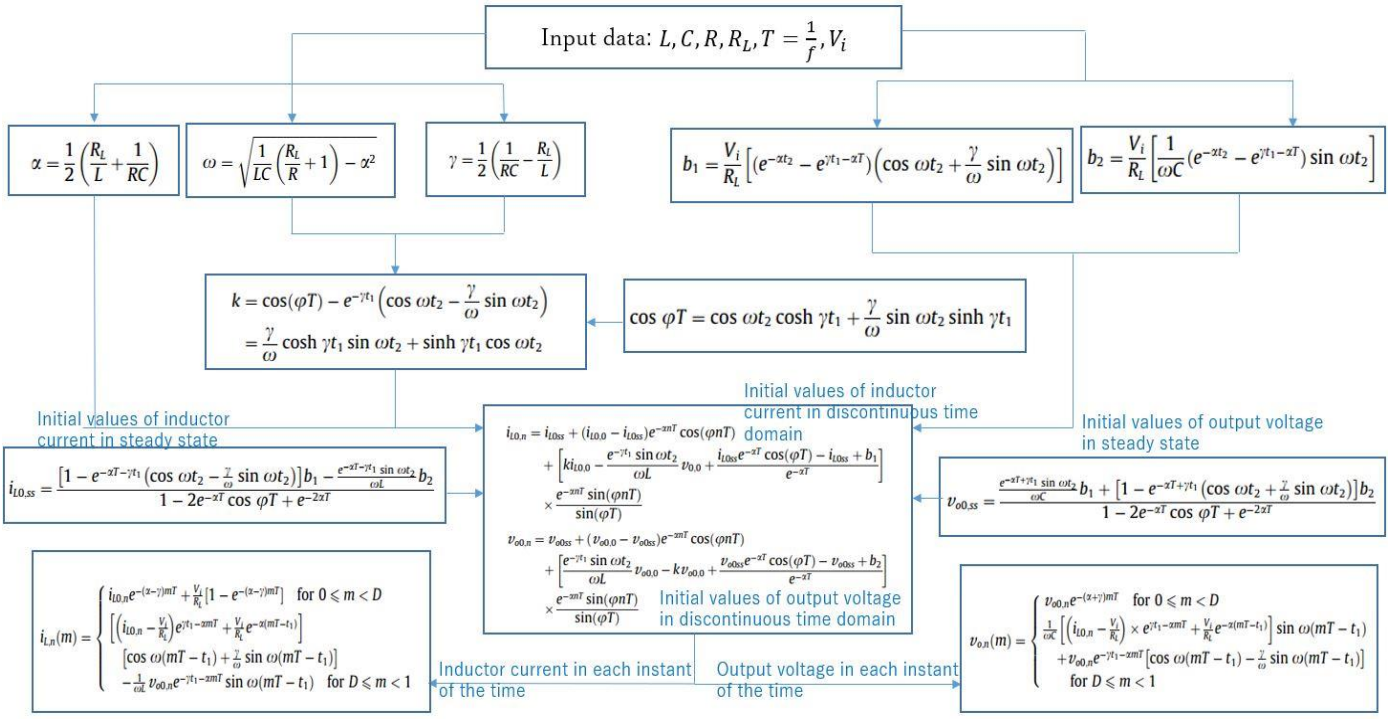

Figure 3.9. Flow chart of buck-boost converter mathematical model.

Where:

L: Inductance (H),

C: Capacitance (F),

R: Resistance (Ω),

R_L: Equivalent resistance of inductor (Ω),

n: The number of switching time intervals,

m: A unit time variable,

T: Switching period,

t_1 means the switch is on, t_2 means the switch is off.

This integrated model can be applied in Continuous Conduction Mode (CCM) and Discontinuous Conduction Mode (DCM). In the application of solar energy, the output voltage of the DC-DC converter is controlled by the duty cycle. The mathematical model of average output voltage versus duty cycle of the buck-boost converter is described as follows [28]:

The initial values of inductor current in steady state at [0, DT]:

$$i_{L0,ss} = \frac{\left[1 - e^{-\alpha T - \gamma t_1}\left(cos\omega t_2 - \frac{\gamma}{\omega} sin\omega t_2\right)\right] b_1 - \frac{e^{-\alpha T - \gamma t_1} sin\omega t_2}{\omega L} b_2}{1 - 2e^{-\alpha T} cos\varphi T + e^{-2\alpha T}} \tag{3.15}$$

The initial values of output voltage in steady state at [0, DT]:

$$v_{o0,ss} = \frac{\frac{e^{-\alpha T + \gamma t_1} sin\omega t_2}{\omega C} b_1 + \left[1 - e^{-\alpha T + \gamma t_1}\left(cos\omega t_2 + \frac{\gamma}{\omega} sin\omega t_2\right)\right] b_2}{1 - 2e^{-\alpha T} cos\varphi T + e^{-2\alpha T}} \tag{3.16}$$

The initial values of inductor current in steady state at [DT, T]:

$$i_{L1,ss} = \left\{\frac{\left[1 - e^{-\alpha T - \gamma t_1}\left(cos\omega t_2 - \frac{\gamma}{\omega} sin\omega t_2\right)\right] b_1 - \frac{e^{-\alpha T - \gamma t_1} sin\omega t_2}{\omega L} b_2}{1 - 2e^{-\alpha T} cos\varphi T + e^{-2\alpha T}}\right\} \times e^{-(\alpha - \gamma) t_1} + \frac{V_i}{R_L} \times \left[1 - e^{-(\alpha - \gamma) t_1}\right] \tag{3.17}$$

The initial values of output voltage in steady state at [DT, T]:

$$v_{o1,ss} = \frac{\frac{e^{-\alpha T + \gamma t_1} sin\omega t_2}{\omega C} b_1 + \left[1 - e^{-\alpha T + \gamma t_1}\left(cos\omega t_2 + \frac{\gamma}{\omega} sin\omega t_2\right)\right] b_2}{1 - 2e^{-\alpha T} cos\varphi T + e^{-2\alpha T}} \times e^{-(\alpha - \gamma) t_1} \tag{3.18}$$

The average value of output voltage is equal with:

$$V_O = \frac{v_{o0,ss}}{(\alpha + \gamma) T}\left(1 - e^{-(\alpha + \gamma) DT}\right) + \frac{i_{L1,ss}}{\omega C}(a_0 a_1 + \omega a_3) + v_{o1,ss}\left[a_0\left(a_2 - \frac{\gamma}{\omega} a_1\right) - a_3(\gamma - \alpha)\right. \tag{3.19}$$

In average output voltage calculation equation, a_0, a_1, a_2, a_3 are defined as:

$$a_0 = \frac{e^{-\alpha t_2}}{(\alpha^2 + \omega^2)T^2} \tag{3.20}$$

$$a_1 = -\alpha T \, sin \, \omega t_2 - \omega T cos \, \omega t_2 \tag{3.21}$$

$$a_2 = -\alpha T \cos \omega t_2 + \omega T \sin \omega t_2 \tag{3.22}$$

$$a_3 = \frac{1}{(\alpha^2 + \omega^2)T} \tag{3.23}$$

By applying these values $V_i = 17V, R = 40\Omega, C = 0.25mF, L = 7mH, and \; f = 1kHz$ in equations (3.15)-(3.19), the variations characteristic curve of average output voltage in steady state versus duty cycle is plotted in Figure 3.10 [28]. In order to confirm the feasibility of this mathematical model, the same parameter values have been applied in MATLAB code; the result is shown in Figure 3.11. The model can be validated by comparing Figure 3.11 with the reference paper [28].

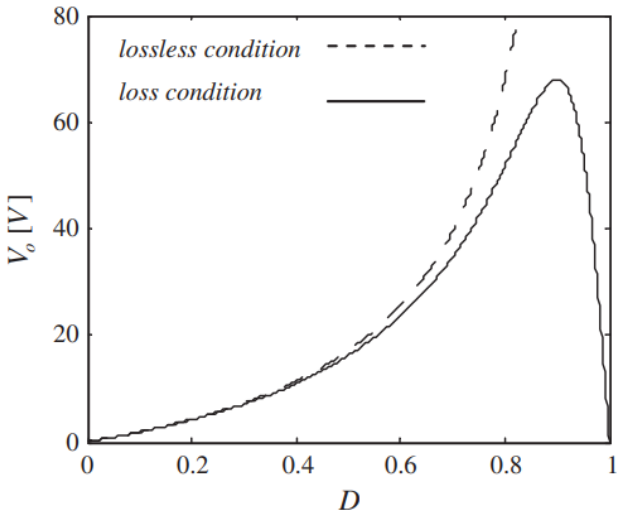

Figure 3.10. Variation curve of average output voltage versus duty cycle from reference (Adapted from [28])

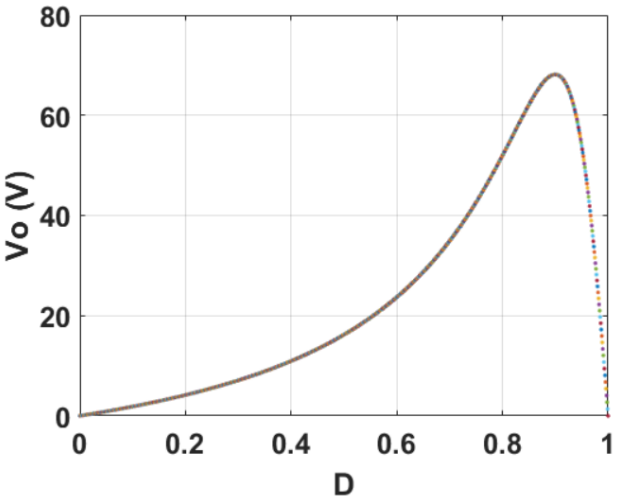

Figure 3.11. Variation curve of average output voltage versus duty cycle result from MATLAB code.

3.3.5. Buck-boost converter design

There is no specific calculation of the inductance and the capacitance required by the power converter with the PV system as the non-linear input source [29]. The most significant design in the DC converter is determining the inductance and capacitance used in the MPPT converters. If the inductance is too small, the dc converter will work in the discontinuous mode. While the inductance is too large, the transient response will become slow. For capacitance, if it is too small, the voltage ripple of the converter becomes large. While the value of capacitance is too large, the response of the converter will also become slow. And not only does the value of parameters influence the performance of the DC converter, but the number and configuration of components also affect the output. Table 3.2. indicates the different parameters' influence on the DC-DC converter's performance.

Table 3.2. Comparison of converter design parameters and effects [30].

Parameter	Perturbation	Cost	Loss	Ripple	Efficiency	Mode of Conduction
Switching Frequency	Increase	high	high	low	high	CCM
	Decrease	high	low	high	low	DCM
Inductance	Increase	high	high	high	N/A	CCM
	Decrease	low	low	low	N/A	DCM
Capacitance	Increase	low	high	low	low	CCM
	Decrease	high	low	high	N/A	DCM
Resistance	Increase	high	high	high	low	CCM/DCM
	Decrease	low	low	low	high	DCM/Non-Operational

Generally, there are two methods that can be used to calculate the inductance of a buck-boost converter:

$$L \geq \frac{V_{in} * D}{f * \Delta i} \tag{3.24}$$

Where Δi is the maximum current ripple.

or

$$L \geq \frac{R_{Lmax} * (1 - D_{min})^2}{2 * f} \tag{3.25}$$

Where R_{Lmax} is the maximum value of load resistance.

The above two inequalities can determine the minimum inductance value in a buck-boost converter.

When coming to the capacitance calculation, inequation (3.26) is introduced below:

$$C \geq \frac{V_o * D}{F * \Delta V_o * R} \tag{3.26}$$

Where:

V_o: Output voltage (V)

ΔV_o: Output voltage ripple

R: Load resistance

For example, design a PWM buck-boost converter used in a PV system that meets the following specifications: $V_I = 30V \pm 2V, V_O = 40V, I_O = 6.5A - 7.5A, f = 15kHz$ is given in Table 3.3.

Table 3.3. Detailed design of a PWM buck-boost converter

$Maximum\ power$:	$P_{Omax} = V_O I_{Omax} = 40V \times 7.5A = 300W$
$Minimum\ power$:	$P_{Omin} = V_O I_{Omin} = 40V \times 6.5A = 260W$
$Minimum\ value\ of\ load\ resistance$:	$R_{Lmin} = \frac{V_O}{I_{Omax}} = \frac{40V}{7.5A} = 5.33\Omega$
$Maximum\ value\ of\ load\ resistance$:	$R_{Lmax} = \frac{V_O}{I_{Omin}} = \frac{40V}{6.5A} = 6.15\Omega$
$Minimun\ dc\ voltage\ transfer\ function$:	$M_{VDCmin} = \frac{V_O}{V_{imax}} = \frac{40}{32} = 1.25$
$Maximun\ dc\ voltage\ transfer\ function$:	$M_{VDCmax} = \frac{V_O}{V_{imin}} = \frac{40}{28} = 1.43$
$Assume\ the\ converter\ efficiency\ \eta = 85\%,\ the\ duty\ cycle$:	$D_{min} = \frac{M_{VDCmin}}{M_{VDCmin} + \eta} = \frac{1.25}{1.25 + 0.85} = 0.595$ $D_{max} = \frac{M_{VDCmax}}{M_{VDCmax} + \eta} = \frac{1.43}{1.43 + 0.85} = 0.627$
$The\ minimum\ inductance$:	$L_{min} = \frac{R_{Lmax}(1 - D_{min})^2}{2f} = \frac{6.15 \times (1 - 0.595)^2}{2 \times 15000} = 33.6\mu H,$ $pick \quad L = 35\mu H$
$Ripple\ voltage\ across\ capacitance$:	$V_{Cpp} = \Delta V_o = 1\% V_{mp} = 1\% \times 30V = 0.3V$
$The\ minimum\ capacitance$:	$C_{min} = \frac{D_{max}}{f R_{Lmin}} * \frac{V_O}{V_{Cpp}} = 1.04mF$

Regarding the negative output voltage of buck-boost converter, there are many ways to deal with this problem. The simplest way is to change the number and configuration of components, such as the diode, switch, etc. For example, a model with two switches and two diodes with positive output voltage

is shown in Figure 3.12.

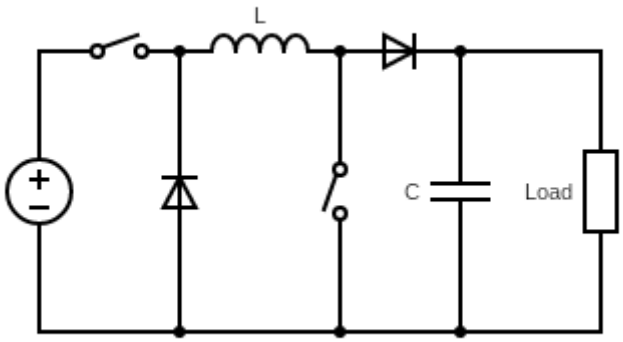

Figure 3.12. The positive output configuration of buck-boost converter [31].

All the calculated values in Table 3.3 were applied in the Simulink model with INC MPPT method measurement, which will be explained in the next section.

3.4. MPPT Simulink model:

A detailed simulation model was performed in MATLAB Simulink to assess the performance of the different MPPTs, shown in Figure 3.13. The model consists of 3 parallel strings; each string includes one PV module composed of 36 cells, the MPPT controller, the DC-DC buck converter, one DC link, and the load. The characteristic electrical specification of the solar panels is given in Table 3.4. The input variables of the simulation model are solar irradiance and cell temperature. The subsystem of the proposed fuzzy logic-based variable step INC is shown in Figure 3.14. The fuzzy logic block produces the proper duty cycle step size, which can be used as the new step size of the incremental conductance method.

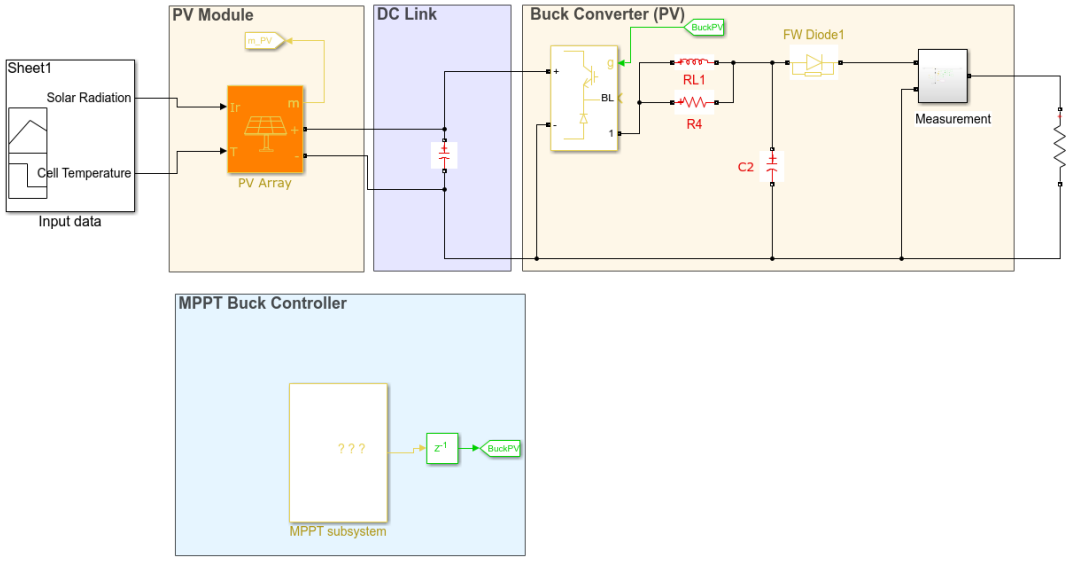

Figure 3.13. PV module Simulink model.

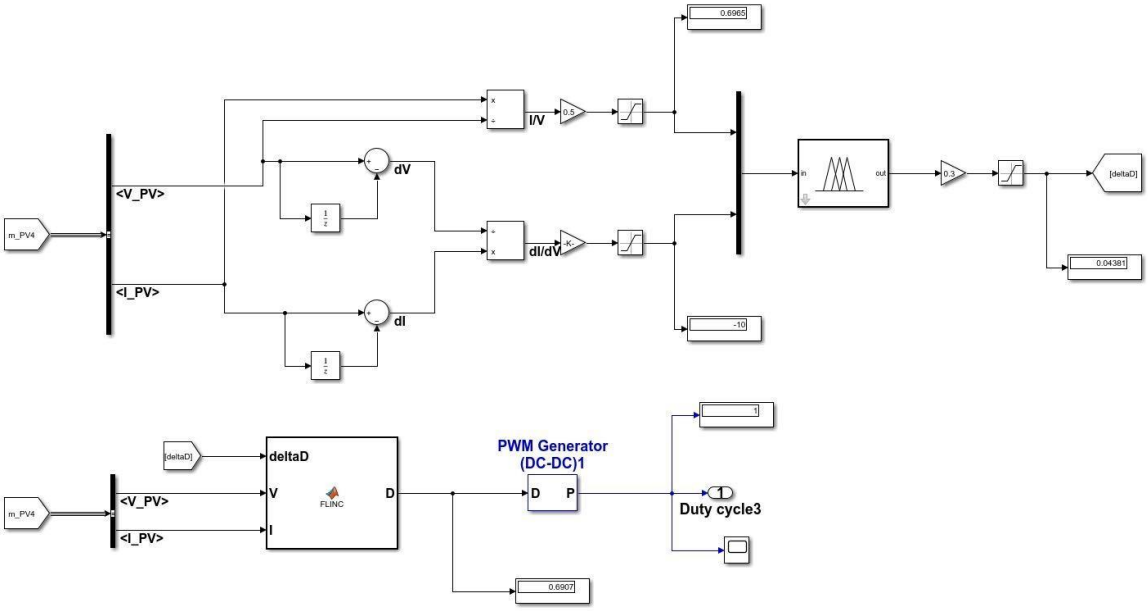

Figure 3.14. Subsystem of fuzzy-logic-based INC.

Table 3.4. Characteristic electrical specifications of the solar panels

Number of cells (N_s)	36
Maximum power (P_{max})	160 [W]
Maximum power voltage (V_{mp})	17.9 [V]
Maximum power current (I_{mp})	8.94 [A]
Open circuit voltage (V_{oc})	21.6 [V]
Short circuit current (I_{sc})	9.47 [A]
Temperature coefficient of V_{oc}	-0.38 [%/℃]
Temperature coefficient of I_{sc}	0.1 [%/℃]

Considering the irradiation change is 0-0.06s: $1000W/m^2$, 0.06s-0.12s: $800W/m^2$, 0.12s-0.18s: $400W/m^2$, and 0.18s-0.24s: $1000W/m^2$. The cell temperature keeps at 25℃. The simulation result is shown in Figure 3.15 below.

It can be found from Figure 3.15 that the novel FL-INC method can track the MPP faster and more accurately. It is obvious that, intelligent control techniques are superior to conventional control techniques. The red line represents INC, the blue one is P&O, the yellow line is fuzzy logic, and the violet one expresses the FL-INC method. When the simulation model starts working, the new FL-INC method can track the MPP at the fastest speed, followed by fuzzy logic, P&O, INC. In addition, FL-INC has less fluctuation and oscillation around MPP at the steady state.

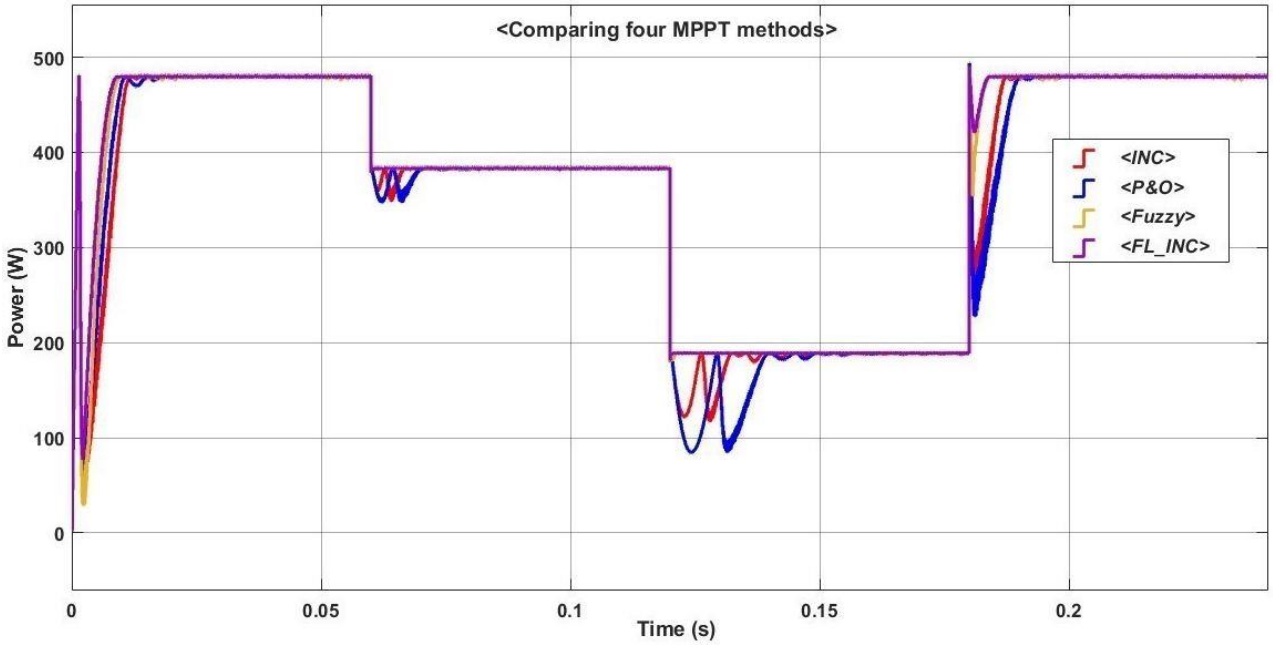

Figure 3.15. Comparison of the simulation results of the four MPPT methods.

Figure 3.16 shows a more transparent and precise comparison between MPPTs methods, considering different modes of steady state, the dramatic reduction in irradiation, and the sharp increase in irradiation. The results emphasize the advantages of reducing the convergence time and improving tracking speed when applying the fuzzy logic variable step INC strategy.

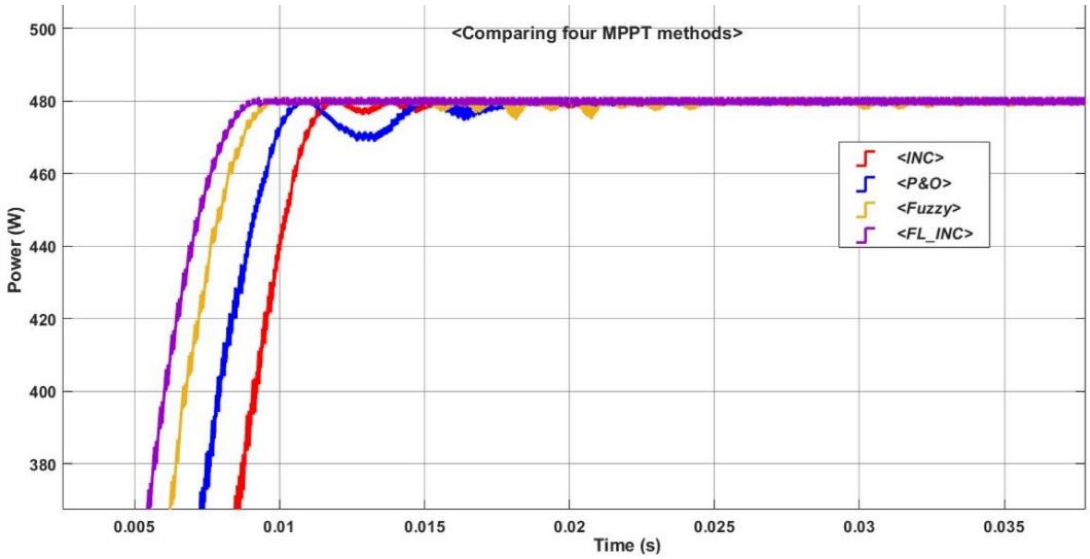

(a)

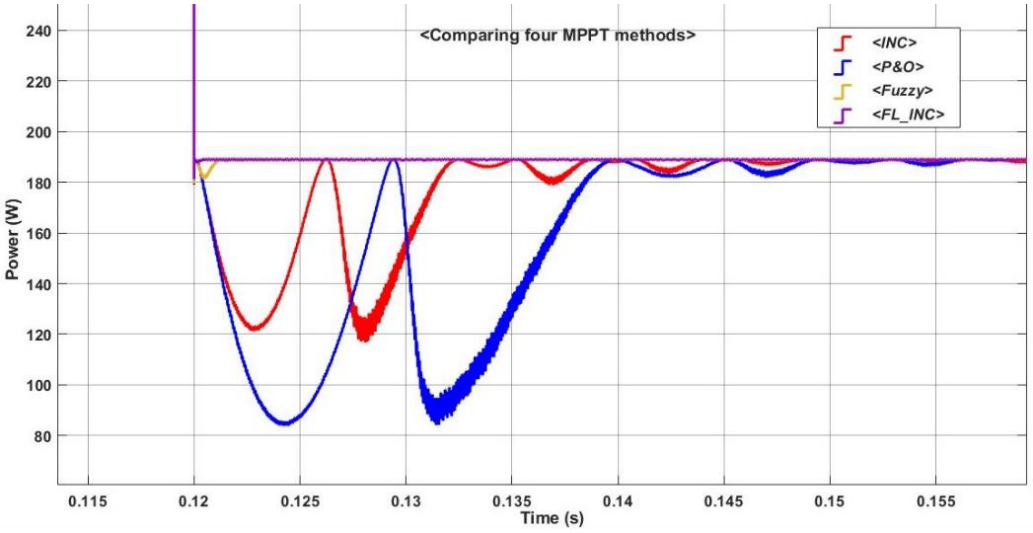

(b)

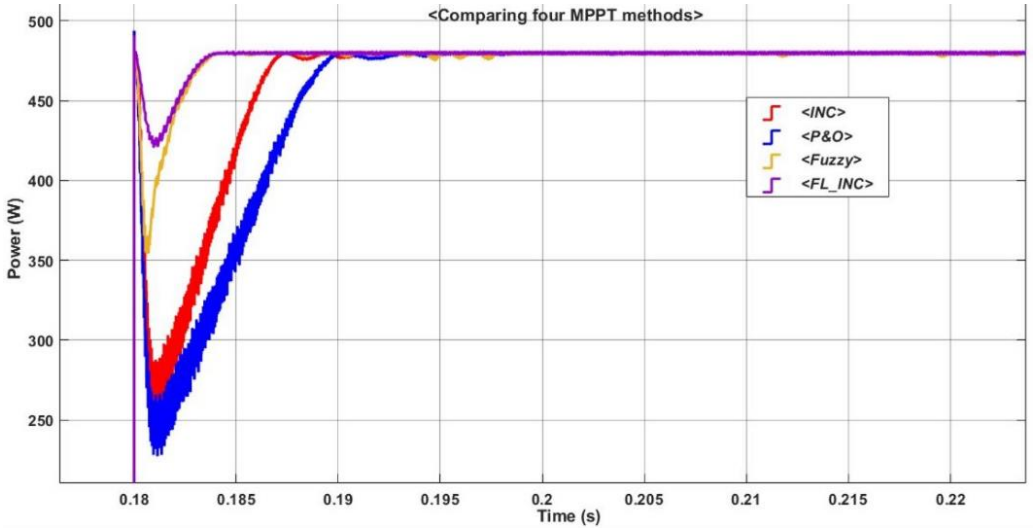

(c)

Figure 3.16. Comparison between the four methods: (a)the first steady state; (b)the dramatic reduction in irradiance; (c)the sharp increase in irradiance.

As shown in Figure 3.16(a), the FL-INC technique can first find the MPP and then work on it with fewer oscillations. Figure 3.16(b) shows that, the FL-INC method is capable of tracking the MPP quickly, in contrast to conventional methods, even when the solar irradiation suddenly declines from $800\,W/m^2$ to $400\,W/m^2$. As indicated in Figure 3.16(c), when the irradiation rises again to $1000W/m^2$, the FL-INC can find the MPP quickly, unlike other methods, especially P&O and INC, which take more time on convergence. Comparing these four MPPT control strategies indicates that FL-INC is better at fast and accurate tracking of the MPP, resulting in additional power out from the PV panel.

In order to estimate how good performance the new FL-INC-based MPPT has, the simulation model was carried out, considering the standard testing condition in which the solar radiation is assumed to be $1000W/m^2$ at 25℃. The results are represented in Figure 3.17. The simulation results revealed that

all four methods gradually stabilized around the maximum power point after 0.025 seconds. But the higher speed and accurate tracking method used in FL-INC-based MPPT provides a 6.29% extra output power in the short time period, compared with the traditional P&O MPPTs. The extra power generated from the FL-INC-based MPPT at the standard test condition compared with other methods is given in Table 3.5.

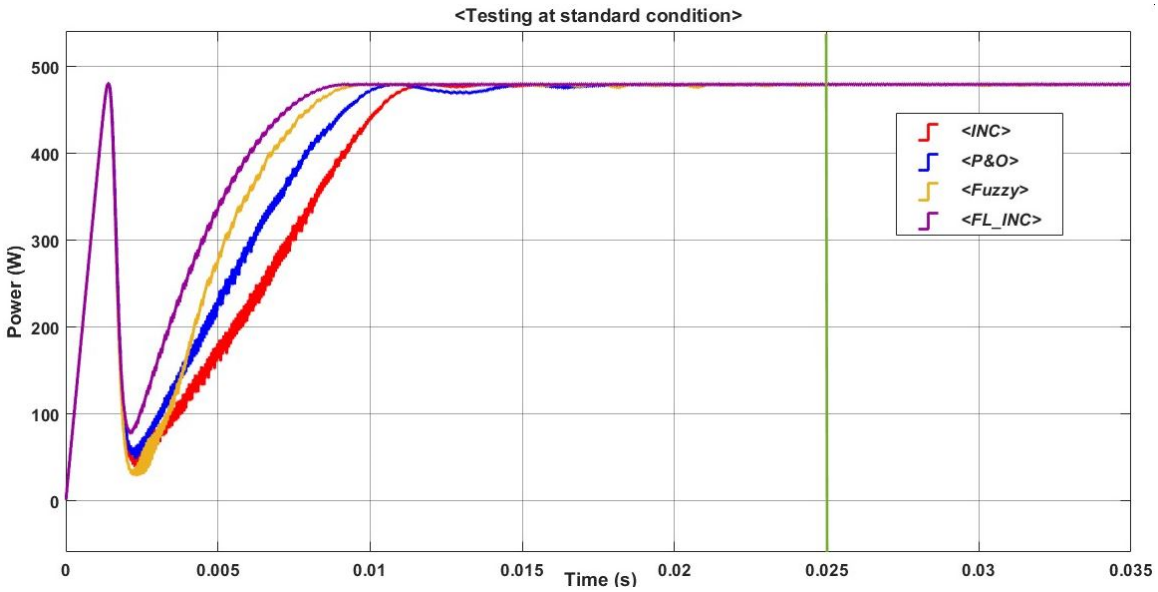

Figure 3.17. Simulation result at standard condition.

When comparing the conventional P&O method with the intelligent fuzzy logic method, The FLC method can generate up to 2.54% more electricity than the P&O method. However, comparing conventional P&O methods with the new FL-INC, the FL-INC method surprisingly generates approximately 2.5 times the extra electricity generation in the general FLC during testing. Based on this result, it is evident that the FL-INC method performs better than the other three MPPT methods.

Table 3.5. Estimation of extra electricity generated in the 0-0.025s from different MPPT methods

Compare P&O with FL-INC	Cumulative Electricity generation	Extra Electricity generation
	P&O: 9.913 Ws	6.29%
	FL-INC: 10.537 Ws	
Compare P&O with FLC	Cumulative Electricity generation	Extra Electricity generation
	P&O: 9.913 Ws	2.54%
	FLC: 10.537 Ws	
Compare FLC with FL-INC	Cumulative Electricity generation	Extra Electricity generation
	FLC: 10.165 Ws	3.65%
	FL-INC: 10.537 Ws	

Chapter 4

Experimental Validation

4.1. Indoor experimental validation

In order to further analyze their respective strengths and weaknesses, the simulation model results for all MPPTs were validated with indoor and outdoor experimental systems. Figure 4.1. shows the standard type solar simulator (Single light type) installed at the Energy and Environmental Systems (EES) laboratory was used to validate the simulation results. The solar simulator uses a high-pressure xenon lamp as a light source with an irradiation intensity of 1 SUN and a spectral distribution similar to sunlight (AM 1.5 G) received on the ground.

Figure 4.1. Standard-type solar simulator installed at the EES lab.

This experimental system consists of a PV cell whose nominal maximum power is 102.318 mW, a

solar radiation producer which can meet the standard testing condition requirements (solar radiation at $1000\ W/m^2$ and cell temperature at 25℃) and a voltage-current source monitor system to generate PV characteristic curve (Figure 4.2).

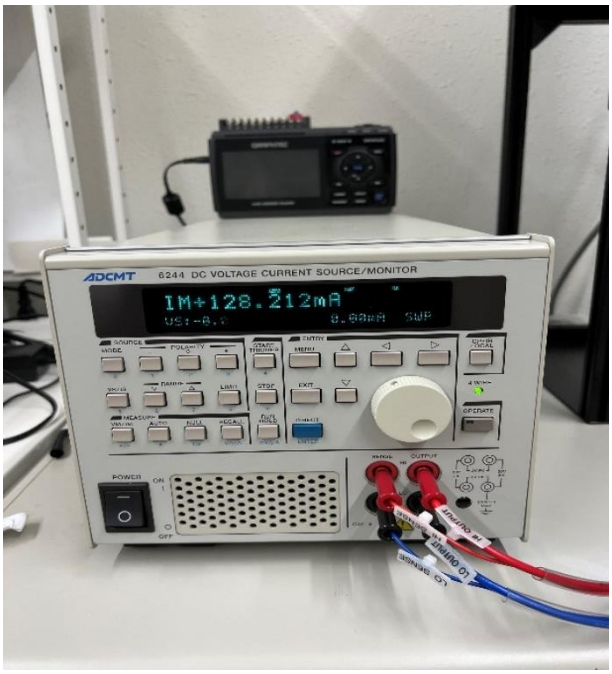

Figure 4.2. Voltage-current source monitor system.

The technical parameters of the testing PV cell are reported in Table 4.1.

Table 4.1. Technical parameters of the testing PV cell.

Number of cells (N_s)	1
Maximum power (P_{max})	102.318 [mW]
Maximum power voltage (V_{mp})	0.4460 [V]
Maximum power current (I_{mp})	229.429 [mA]
Open circuit voltage (V_{oc})	0.5694 [V]
Short circuit current (I_{sc})	246.910 [mA]
Series resistance (R_s)	239.788 [$m\Omega$]
Shunt resistance (R_{sh})	13.108 [Ω]

From Table 4.1, it is clear that the testing cell is a very small solar cell whose rated maximum power is just 0.102 W. Based on these parameters given above, the experimental result is shown in Figure

4.3. To validate the simulation model results, the same parameters' values have been applied in MATLAB/Simulink to compare with it.

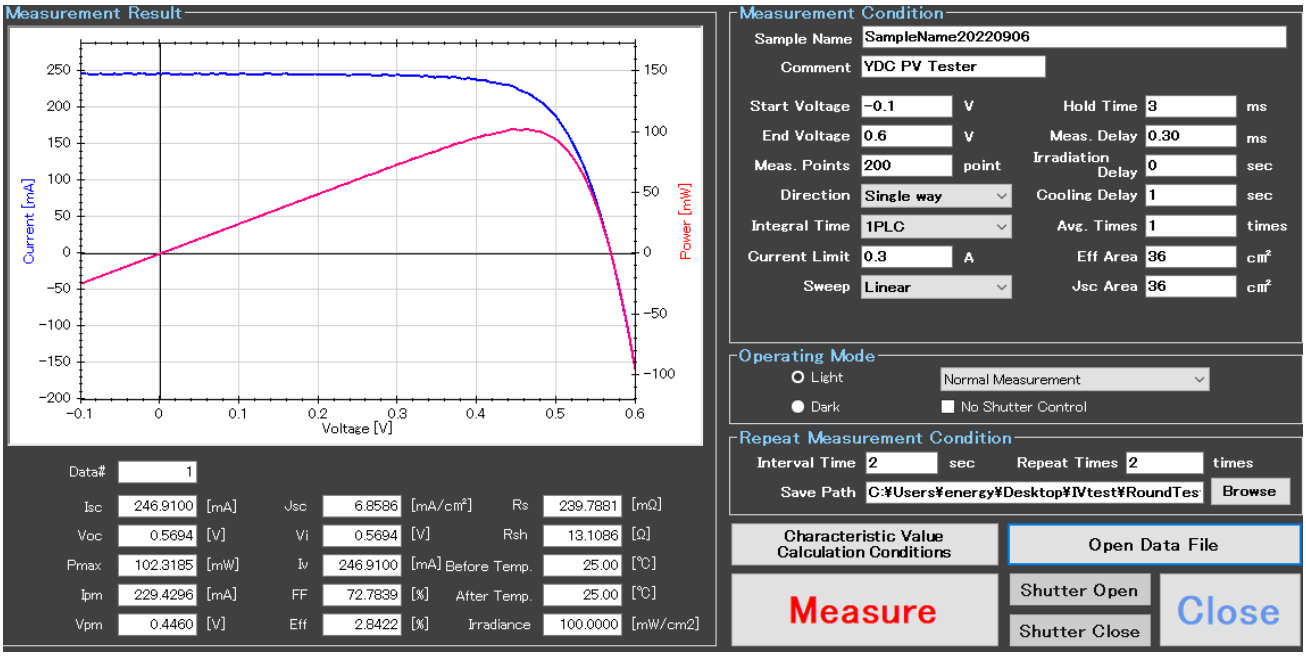

Figure 4.3. I-V curve of the standard cell based on the measured data.

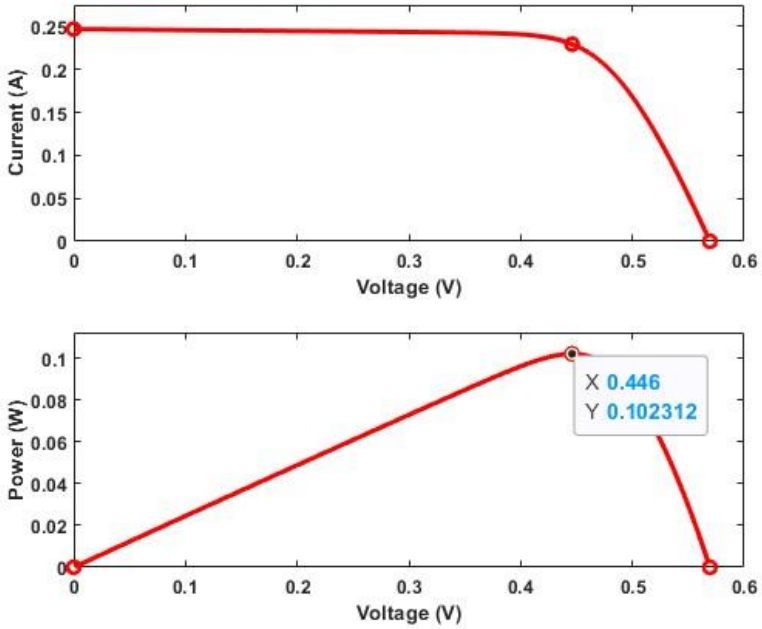

Figure 4.4. PV characteristic curve extracted from the Simulink model.

Comparing the experimental result with the Simulink result, the accuracy of the experimental setup is verified.

The results of the simulation model for all four different MPPT methods (Perturb and Observe (P&O), Incremental Conductance (INC), Fuzzy Logic (FLC), and Fuzzy-logic based INC (FL-INC))

are shown in Figure 4.5. Obviously, in this figure, all of the MPPT methods tracked the MPP precisely within a short time. However, the novel FL-INC method can track the MPP faster and more accurately, even for the low nominal power of 0.1023 W.

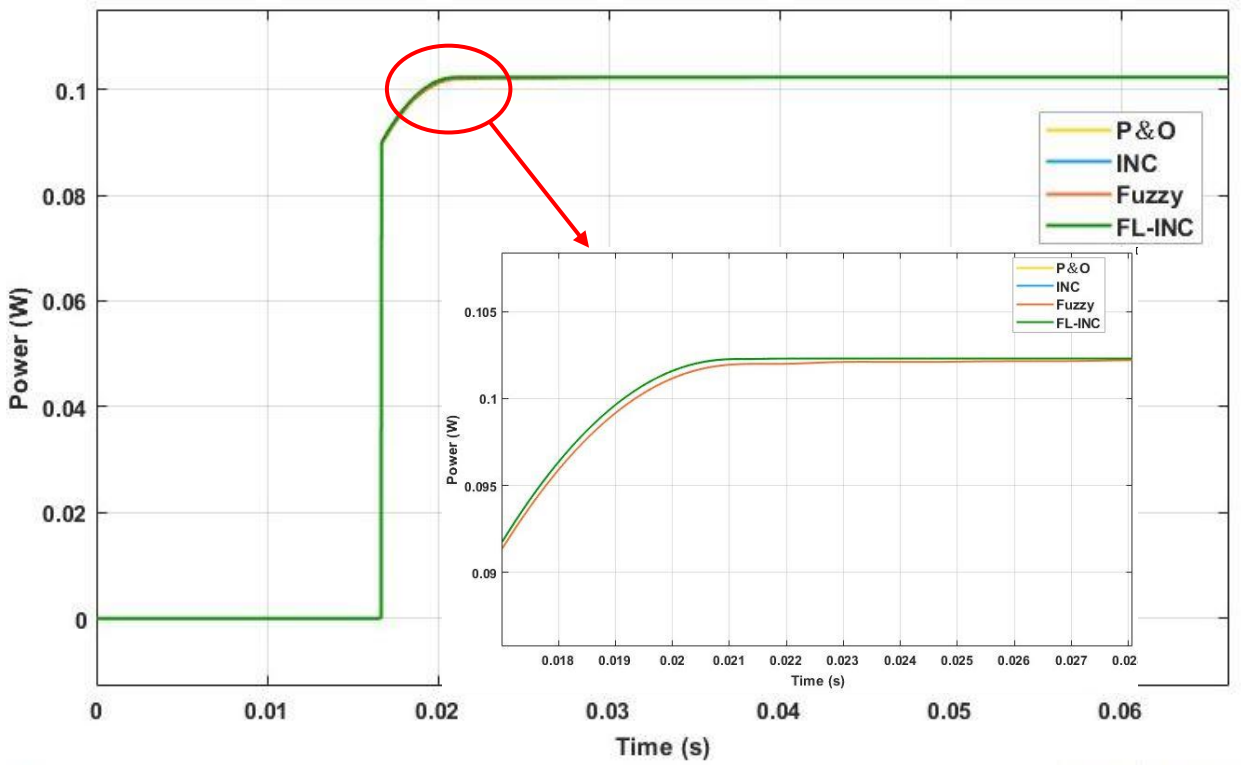

Figure 4.5. Results of four MPPT methods in Simulink.

4.2. Outdoor experimental validation:

The outdoor experimental system installed at Chikushi campus, Kyushu University, consists of three PV parallel panels with nominal power of 160 W for each, a MS-40S Pyranometer to measure the incident solar radiation on the tilted PV surface, a LM335 temperature sensor, and a data acquisitor to collect the values of current, voltage, power, and operating temperature (see Figure 4.6).

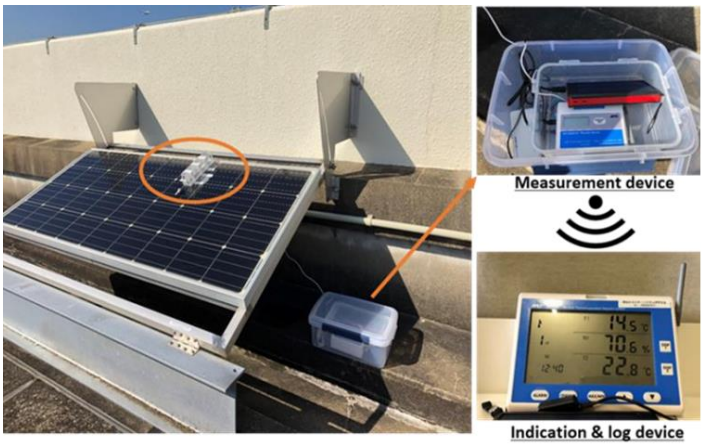

Figure 4.6. Outdoor experimental system.

The data measured on solar irradiation and PV output power for eniter one year was used in the simulation model to validate the results. The data on ambient temperature was collected from the Japan Meteorological Agency [32]. It is worth noting that the temperature measured by the meteorological agency can not be used directly because what can be recognized in Simulink is cell temperature. Cell temperature will be affected by the intensity of solar radiation and wind speed; there is an equation that is established for cell temperature [33]:

$$T_{cell} = 0.943 \times T_a + 0.028 \times G_S - 1.528 \times S_w + 4.3 \quad (4.1)$$

Where:

T_a: Ambient temperature (℃)

G_s: Solar irradiance (W/m^2)

S_w: Wind speed (m/s)

In this study, only solar irradiance greater than 100 W/m^2 was used in the analysis because when solar irradiance is lower than 100 W/m^2 the MPPT controller can't work well, and the output power is very small. Figure 4.7 represents the solar radiation on the PV panel's surface and cell temperature at 12 am on July 22nd in, 2020. Figure 4.8 shows the simulation result of the different MPPT methods in this research for a short period of ten minutes of simulation on this summer sunny day. As shown in Figure 4.8, the FL-INC method extracts more power with higher speed and less fluctuation than the P&O method. The hourly estimation of the PV module output power is reported in Table 4.2. The New FL-INC method has better performance than other MPPT methods.

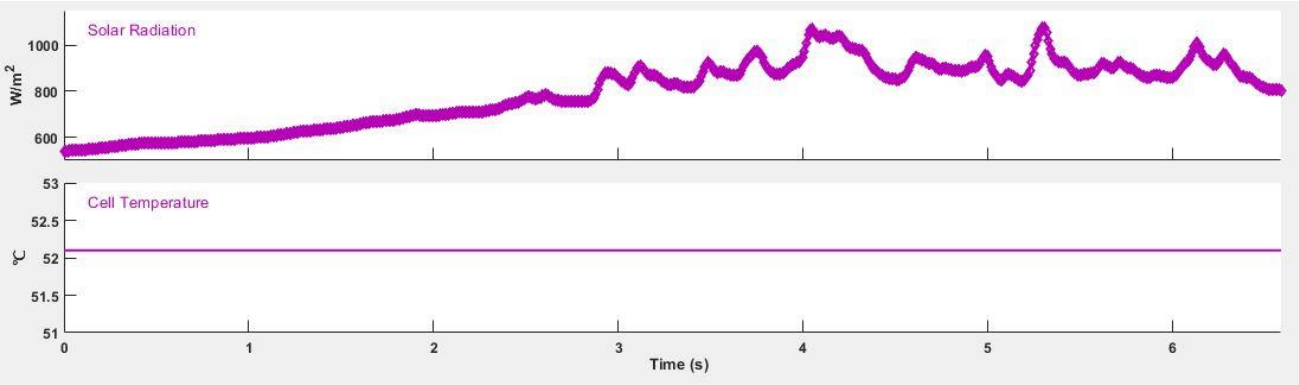

Figure 4.7. Solar radiation and cell temperature at 12 am on July 22nd in 2020.

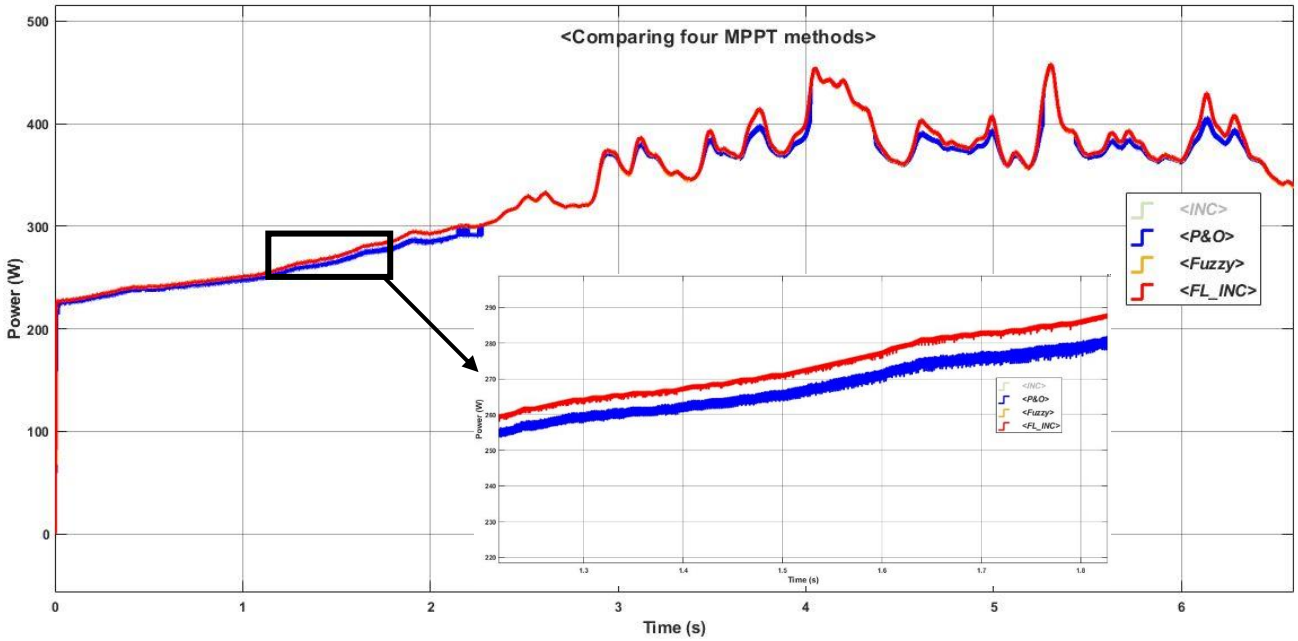

Figure 4.8. PV output power in different MPPT at 12 am on July 22nd.

Table 4.2. One day simulation results on July 22nd.

Time	Solar Radiation $[W/m^2]$	Cell temperature [℃]	P&O $[Wh]$	Fuzzy $[Wh]$	FL-INC $[Wh]$	Extra $[Wh]$
7:00	113.9	31.4091	47.80	49.22	49.76	P&O with FL-INC: 2.04%
8:00	308.3	37.5386	134.12	135.95	136.38	
9:00	511.1	44.2089	219.54	222.18	222.46	
10:00	694.4	50.0957	288.85	295.83	296.15	
11:00	838.9	52.0872	349.55	354.60	355.12	P&O with FLC: 1.93%
12:00	941.7	54.4976	387.11	393.72	393.95	
13:00	958.3	55.1283	390.89	399.47	399.40	
14:00	922.2	52.8593	381.98	388.66	388.93	
15:00	838.9	49.8441	352.94	358.60	358.92	FLC with FL-INC: 0.10%
16:00	669.4	44.9776	285.76	292.14	292.10	
17:00	366.7	31.8394	162.48	167.19	167.46	
18:00	219.4	35.768	92.75	96.02	96.34	
Total Power $[Wh]$			3093.77	3153.58	3156.97	

The simulation result in different climatic conditions and time periods is shown in Figure 4.9 and Figure 4.10. One cloudy winter day (October 7th, 2020) was selected to conduct the analysis. The solar irradiance and temperature on this day are lower than in July. The hourly estimation is shown in Table 4.3. As can be seen from the results, even on cloudy days with lower solar radiation, the new FL-INC method has better performance than other MPPT methods.

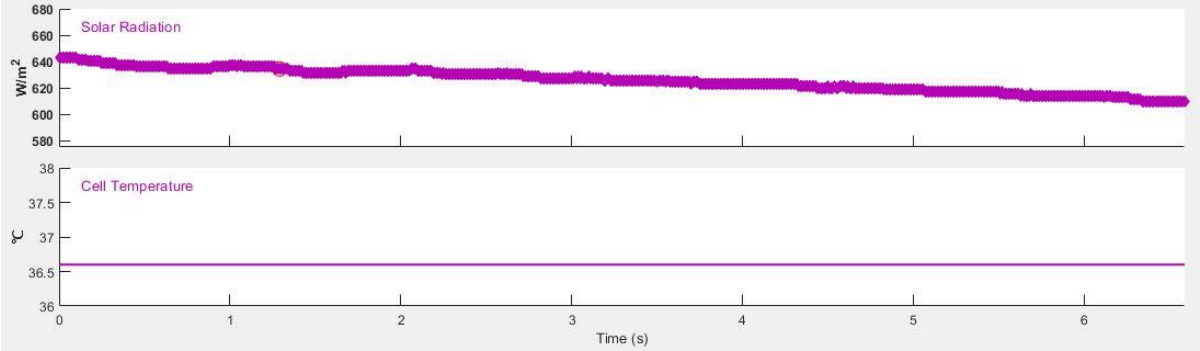

Figure 4.9. Solar radiation and cell temperature at 14pm on October 7th in 2020.

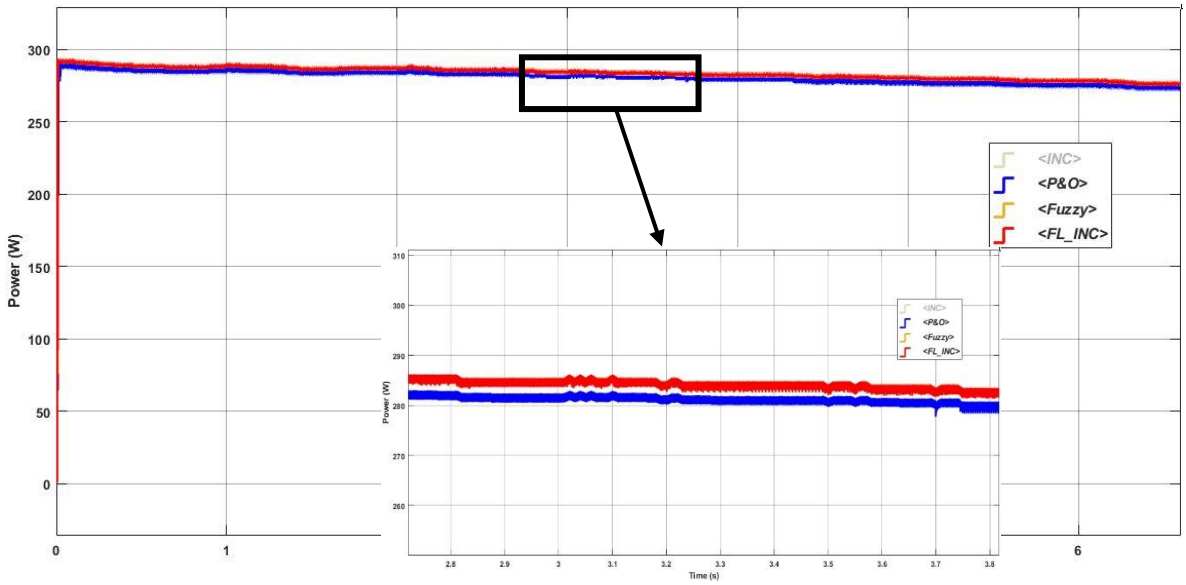

Figure 4.10. PV output power in different MPPT at 14 pm on October 7th.

Table 4.3. 1-day simulation results on October 7th.

Time	Solar Radiation $[W/m^2]$	Cell temperature [℃]	P&O $[Wh]$	Fuzzy $[Wh]$	FL-INC $[Wh]$	Extra $[Wh]$
8:00	——					P&O with FL-INC: 2.13%
9:00	197.2	28.3245	82.33	89.11	89.20	
10:00	366.7	33.2399	163.52	166.36	166.48	
11:00	491.7	38.9996	215.54	219.16	219.24	
12:00	461.1	38.4973	202.78	205.61	205.63	P&O with FLC: 2.09%
13:00	444.4	37.4089	194.02	198.87	198.96	
14:00	586.1	37.4491	262.06	264.43	264.48	
15:00	411.1	31.476	184.87	188.57	188.64	
16:00	350	32.6099	156.32	158.85	158.94	FLC with FL-INC: 0.04%
17:00	172.2	28.3108	74.81	77.34	77.40	
18:00	——					
19:00	——					
Total Power $[Wh]$			1536.25	1568.30	1568.97	

The simulation model was carried out, for the selected days of the year, considering different climate conditions in each month (see Table 4.4). The analysis result for the one-year simulation is summarized in Table 4.5. The result revealed that the fuzzy logic method could obtain approximately 2.04% more accumulative power than the conventional P&O. When the fuzzy-logic-based variable step INC method is compared with the conventional P&O method, the FL-INC method is able to generate 2.12% more accumulative power than general fuzzy logic method.

Table 4.4. Selected date in this study.

Sunny days	**Cloudy days**
January 25th	January 11th
February 19th	February 5th
March 25th	March 6th
April 7th	April 21st
May 7th	May 17th
June 2nd	June 5th
July 22nd	July 11th
August 30th	August 28th
September 8th	September 23rd
October 6th	October 7th
November 4th	November 28th
December 28th	December 10th

Table 4.5. One-year simulation results.

Time	P&O Power ($\boldsymbol{kWh}$)	Fuzzy Power ($\boldsymbol{kWh}$)	FL-INC Power ($\boldsymbol{kWh}$)	Difference of P&O, Fuzzy ($\boldsymbol{kWh}$)	Saving (%)	Difference of P&O, FL-INC ($\boldsymbol{kWh}$)	Saving (%)
January	31.80	32.36	32.37	0.56	1.76%	0.57	1.79%
February	44.98	45.82	45.83	0.84	1.87%	0.85	1.89%
March	55.65	56.77	56.79	1.12	2.01%	1.14	2.05%
April	65.83	67.61	67.64	1.78	2.70%	1.81	2.75%
May	68.80	70.03	70.14	1.23	1.79%	1.34	1.95%
June	61.71	62.91	63.06	1.2	1.95%	1.35	2.19%
July	33.18	33.91	33.94	0.73	2.20%	0.76	2.29%
August	55.56	56.63	56.66	1.07	1.93%	1.1	1.98%
September	50.04	51.16	51.21	1.12	2.24%	1.17	2.34%
October	59.53	60.77	60.79	1.24	2.08%	1.26	2.12%
November	37.95	38.63	38.65	0.68	1.79%	0.7	1.84%
December	26.47	26.97	26.98	0.5	1.89%	0.51	1.93%
Total power	**591.50**	**603.57**	**604.06**	**12.07**	**2.04%**	**12.56**	**2.12%**

Chapter 5

Conclusion

This research introduced a novel fuzzy-logic-based Incremental Conductance (FL-INC) variable step size MPPT technique to track the maximum power point of the photovoltaic systems in the real indoor experimental system and outdoor setup, whose performance is also compared with conventional Perturb and Observe (P&O) method, Incremental Conductance (INC) method, and intelligent Fuzzy Logic (FLC) method. To this aim, a simulation model was developed in MATLAB/Simulink, which included three main parts: 1) detailed PV output electric power simulation, 2) four MPPT methods, and 3) the buck-boost DC-DC converter that can be used in the system in order to optimize the PV out voltage, based on the corrected the duty cycle values generated by the MPPT.

First, the validation of the simulation results with the indoor experimental system revealed that even if the nominal power is very low, the new FL-INC method can track the maximum power faster and more accurately than other methods. The excellent performance of the FL-INC method also can be seen from the comparison in Simulink with different solar irradiance changes; when the solar radiation has a gradual decrease or sharp increase.

Second, the validation of the results with the outdoor setup installed in Chikushi Campus, using the one-year real measured solar radiation data and temperature, emphasized the superiority of the intelligent MPPT performance over the conventional hill climbing method with approximately 2% extra output power in one year. Compared to existing commercial systems on the market, the proposed MPPT can realize an extra 12.56 kWh of electricity per year from each kilowatt of installed capacity of solar panels on the Chikushi campus. While costs are important, the advantage of using such MPPT is that it can facilitate the rapid deployment of hybrid renewable-based microgrids in the residential sector in Japan.

Future work could concentrate on developing other intelligent and advanced MPPT methods to improve control accuracy, speed, and stability in renewable energy systems. The aim is to obtain more output power with less power loss.

References

[1] Y. Unal, K. Ali, B. Selim. PV system fuzzy logic MPPT method and PI control as a charge controller, Renewable and Sustainable Energy Reviews. 81 (2018) 994-1001.

[2] Farzaneh. H. Ushering in a new age of urban energy efficiency and low emission societies, IEICES. (2021).

[3] Our World in Data: https://ourworldindata.org/grapher/ (accessed November 10, 2022)

[4] R.A. Carlos, L.F. Roberto, O.C. Adalberto. Implementation of a cost-effective fuzzy MPPT controller on the Arduino board, International Journal on Smart Sensing and Intelligent Systems. 11 (2018).

[5] O. Zarrad, M.A. Hajjaji, A. Jemaa and M.N. Mansouri. Sizing control and hardware implementation of a hybrid wind-solar power system, based on an ANN approach, for pumping water, International Journal of Photoenergy. (2019).

[6] P. Nopporn, P. Suttichai, S. Yosanai. Maximum power point tracking using adaptive fuzzy logic control for grid-connected photovoltaic system, Renewable Energy. 30 (2005) 1771-1788.

[7] Shaqour. A, Farzaneh. H, Yoshida. Y, Hinokuma. T. Power control and simulationn of a building integrated stand-alone hybrid PV-wind-battery system in Kasuga City, Japan. Energy Reports. 6 (2020) 1528-1544.

[8] Oussalem. O, Kourchi. M, Rachdy. A, Ajaamoum. M, et al. A low cost controller of PV system based on Arduino board and INC algorithm. Materials Today. 24 (2020) 104-109.

[9] Motahhir. S, Hammoumi. A E, Ghzizal. A E. Photovoltaic system with quantitative comparative between an improved MPPT and existing INC and P&O methods under fast varying of solar irradition. Energy Reports. 4 (2018) 341-350.

[10] Banu. I V, Beniuga. R, Istrate. M. Comparative analysis of the perturb-and-observe and incremental conductance MPPT methods. The 8th International Symposium on Advanced Topics in Electrical Engineering. (2013)

[11] Mahamudul. H, Saad. M, Henk. M I. Photovoltaic system modeling with fuzzy logic based maximum power point tracking algorithm. International Journal of Photoenergy. (2013). http://dx.doi.org/10.1155/2013/762946

[12] Algarin. C R, Fuentes. R L, Castro. A O. Implementation of a cost-effective fuzzy MPPT controller on the Arduino board. International Journal on Smart Sensing and Intelligent systems. Vol. 11 (2018).

[13] Noman. A M, Addoweesh. K E, Mashaly. H M. A fuzzy logic control method for MPPT of PV systems. Conference Paper. (2012)

[14] Kamran. M, Mudassar. M, Fazal. M R, Asghar. M U, et al. Implementation of improved Perturb & Observe MPPT technique with confined search space for standalone photovoltaic system. Journal of King Saud University. 32 (2020) 432-441.

[15] Rahim. N A, Amir. A, Selvaraj. J. Modified Incremental Conductance MPPT with direct control and dual scaled adaptive step-size methods. 4th IET Clean Energy and Technology Conference. (2016).

[16] Upendar. J, Samhith. Y K, Kamal. A K. Modeling and analysis of thevenin and variable step size Incremental Conductance methods to improve the performance of PV system. Fourth International Conference on Electronics. (2020)

[17] Motahhir. S, Chalh. A, Ghzizal. A E, Derouich. A. Development of a low-cost PV system using an improved INC algorithm and a PV panel Proteus model. Journal of Cleaner Production. 204 (2018) 355-365.

[18] Zarrad. O, Hajjaji. M A, Jemaa. A and Mansouri. M N. Sizing control and hardware implementation of

a hybrid wind-solar power system, Based on an ANN approach, for pumping water. International Journal of Photoenergy. (2019). https://doi.org/10.1155/2019/5672032

[19] De Brito, Galotto. L, Sampaio. L P, et al. Evaluation of the main MPPT techniques for photovoltaic applications. IEEE Transactions on Industrial Electronics, vol. 60, No. 3,. (2013)

[20] Liu. C, Wu. B and Cheng. R. Advanced algorithm for MPPT control of photovoltaic systems. Canadian Solar Buildings Conference Montreal. August 20-24 (2004)

[21] Stanford Encyclopedia of Philosophy: https://plato.stanford.edu/entries/logic-fuzzy/

[22] Motahhir. S, Chalh. A, Ghzizal. A E, et al. Modeling of photovoltaic panel by using proteus. Journal of Engineering Science and Technology Review. 10 (2) (2017) 8-13.

[23] Ali. M N, Mahmoud. K, Lehtonen. M and Darwish. M. An efficient fuzzy-logic based variable-step incremental conductance MPPT method for grid-connected PV systems. IEEE Access. (2021)

[24] Hinokuma. T, Farzaneh. H, Design and development of a hybrid renewable energy system using fuzzy logic controller for maximum power point tracking. Kyushu University. (2021)

[25] Mohammed. M and Alibaba. H Z. The effect of photovoltaic (PV) panel tilt angle for best energy generation in hot climate. International Journal of Civil and Structural Engineering Research. 6 (2) (2018) 185-196.

[26] Noman. A, Addoweesh. K, Mashaly. H. A fuzzy logic control method for MPPT of PV systems. Conference Paper. (2012)

[27] K. Kazimierczuk. M. Pulse-Width Modulated DC-DC Power Converters (Second Edition). WILEY. (2016)

[28] Mahery. H M, Babaei. E. Mathematical modeling of buck-boost dc-dc converter and investigation of converter elements on transient and steady state response. Electrical Power and Energy Systems 44 (2013) 949-963.

[29] Ayop. R, Tan. C W. Design of boost converter based on maximum power point resistance for photovoltaic applications. Solar Energy 160 (2018) 322-335.

[30] Iqbal. S M, Mekhilef. S, Soin. N and Omar. R. Buck and boost converter design optimization parameters in modern VLSI technology. IEEE. (2011)

[31] Zaghba. L, Borni. A, Bouchakour. A and Terki. N. Buck-boost converter system modeling and incremental inductance algorithm for photovoltaic system via Matlab/Simulink. Revue des Energies Renouvelables SIENR'14 (2014) 63-70.

[32] Japan Meteorological Agency: https://www.data.jma.go.jp/gmd/risk/obsdl/index.php

[33] TamizhMani. G, Ji. L, Tang. Y and Petacci. L. Photovoltaic module thermal/wind performance: Long-term monitoring and module development for energy rating. NCPV and solar program review meeting. (2003) 936.